COURSE 6

SEISMIC NUMERICAL MODELING

D. KOSLOFF AND D. KESSLER

Department Of Geophysics And Planetary Sciences, Raymond & Beverly Sackler Faculty Of Exact Sciences, Tel Aviv University, Tel Aviv, Israel, 69978.

Y. Desaubies, A. Tarantola and J. Zinn-Justin, eds.
Les Houches, Session L, 1988
Tomographie Océanographique et Géophysique / Oceanographic and Geophysical Tomography

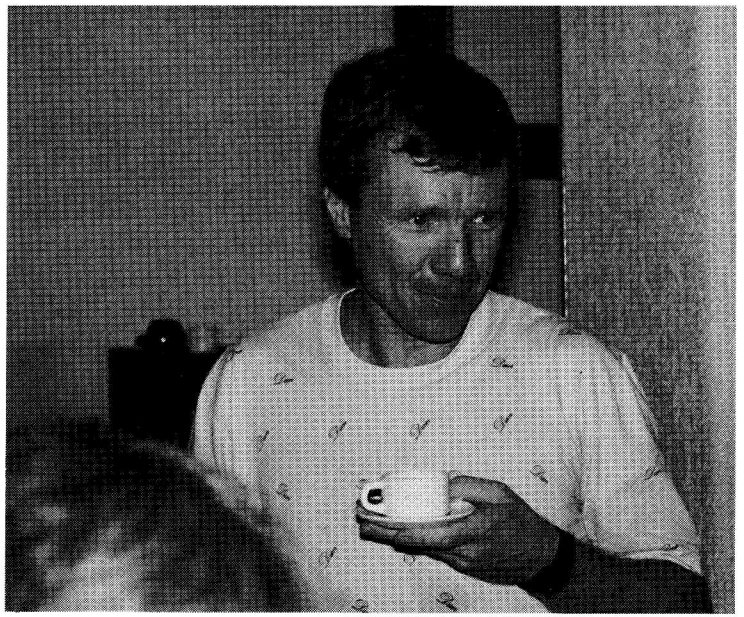

Contents

Introduction

The objective of seismic forward modeling can be stated as: "given an assumed structure of the subsurface, predict what geophones of a seismic survey over that structure would record". Seismic modeling is a valuable tool for seismic interpretation as well as an essential ingredient in seismic inversion algorithms.

All types of seismic forward modeling are based on some solution of a governing wave equation. Presently one can distinguish between three main types of forward modeling namely, analytical methods, geometrical optics methods (Ray Tracing), and direct methods (e.g. finite differences, finite elements, the Fourier method).

Analytical methods are based on closed form solutions of the governing wave equation. They are limited to simple structures because only then closed form solutions exist. Because of their high accuracy they can serve as a standard for testing other methods. For multilayer structures the solutions often include integrals with singularities (e.g. the reflectivity method). These integrals need to be carried out numerically with caution, and in such a case the methods should be considered only semi analytical.

Geometrical optics methods are a high frequency approximation which most commonly is based on the ray series. These methods are generally very fast and effective for getting travel time information. However, they do not always give correct amplitudes or explain non geometrical optics phenomena (e.g. tunneling). For complicated structures or when many multiples and converted phases need to be accounted for they can become very cumbersome.

Direct methods are based on a direct solution of the equations of motion after approximating the region of propagation by a numerical grid. Direct methods usually do not have restrictions on material variability. In principle they can be very accurate when a sufficiently fine grid is used. However, these methods are expensive, or equivalently, they possess a high frequency limit on resolution. Unlike the first two methods, direct methods produce snapshots with ease, which can be an important aid in interpretation.

In the following we examine a number of direct methods which are currently used in seismology. In the first sections we introduce most of the concepts through the simple example of the one dimensional acoustic wave equation. Next the results will be generalized to acoustic and elastic wave propagation in two and three dimensions. Finally we will discuss some new

approaches for accurate and efficient time integration.

1. One dimensional acoustic wave propagation

1.1. The one dimensional acoustic wave equation

We consider the one dimensional acoustic wave equation for constant density:

$$\frac{1}{c^2}\frac{\partial^2 P}{\partial t^2} = \frac{\partial^2 P}{\partial x^2} \tag{1.1.1}$$

where, x is a Cartesian coordinate, t is the time, $c(x)$ is the acoustic velocity and P is the pressure. The finite difference solution of (1.1.1) uses both temporal and spatial discretizations. Let $\mathrm{d}x$ be the spatial grid size and $\mathrm{d}t$ the time step size. For representing variables we adopt the notation:

$$P_j^n = P(x = x_0 + j\,\mathrm{d}x, t = n\,\mathrm{d}t)$$

and

$$c_j = c(x = x_0 + j\,\mathrm{d}x), \qquad j = 0, \ldots, N_x - 1$$

where N_x is the number of grid points.

1.2. The finite difference approximation

The finite difference second derivative approximation is given by:

$$\frac{\partial^2 P_j^n}{\partial x^2} = \frac{P_{j+1}^n - 2P_j^n + P_{j-1}^n}{\mathrm{d}x^2} \tag{1.2.1}$$

The justification for (1.2.1) can be seen through performing the derivative in two stages:

$$\frac{\partial P_{j+1/2}^n}{\partial x} = \frac{P_{j+1}^n - P_j^n}{\mathrm{d}x}, \tag{1.2.2}$$

and

$$\frac{\partial^2 P_j^n}{\partial x^2} = \frac{\frac{\partial P_{j+1/2}^n}{\partial x} - \frac{\partial P_{j-1/2}^n}{\partial x}}{\mathrm{d}x}. \tag{1.2.3}$$

For the second time derivative we use the same type of approximation:

$$\frac{\partial^2 P_j^n}{\partial t^2} = \frac{P_j^{n+1} - 2P_j^n + P_j^{n-1}}{\mathrm{d}t^2} \tag{1.2.4}$$

A substitution of (1.2.1) and (1.2.4) into (1.1.1) and rearrangement of terms finally yields the scheme:

$$P_j^{n+1} = 2P_j^n - P_j^{n-1} + \frac{c_j^2\,\mathrm{d}t^2}{\mathrm{d}x^2}\left[P_{j+1}^n - 2P_j^n + P_{j-1}^n\right] \tag{1.2.5}$$

This equation comprises an extrapolation where values at time $t = (n+1)\,\mathrm{d}t$ are obtained from values at times $n\,\mathrm{d}t$ and $(n-1)\,\mathrm{d}t$, previously calculated. Boundary conditions at grid points $j = 0$ and $j = N_x - 1$ need to be specified.

1.3. Accuracy

We shall test the spatial derivative approximation for $P = 1$, x, x^2, x^3,...

$$\begin{aligned}
P = 1\text{:}\ & \frac{P_{j+1}^n - 2P_j^n + P_{j-1}^n}{\mathrm{d}x^2} = 0 \\
P = x\text{:}\ & \frac{P_{j+1}^n - 2P_j^n + P_{j-1}^n}{\mathrm{d}x^2} = \frac{(j+1)\,\mathrm{d}x - 2j\,\mathrm{d}x + (j-1)\,\mathrm{d}x}{\mathrm{d}x^2} = 0 \\
P = x^2\text{:}\ & \frac{P_{j+1}^n - 2P_j^n + P_{j-1}^n}{\mathrm{d}x^2} = \frac{(j+1)^2\,\mathrm{d}x^2 - 2j^2\,\mathrm{d}x^2 + (j-1)^2\,\mathrm{d}x^2}{\mathrm{d}x^2} \\
& \qquad = 2 = \frac{\partial^2}{\partial x^2}(x^2) \\
P = x^3\text{:}\ & \frac{P_{j+1}^n - 2P_j^n + P_{j-1}^n}{\mathrm{d}x^2} = \frac{(j+1)^3\,\mathrm{d}x^3 - 2j^3\,\mathrm{d}x^3 + (j-1)^3\,\mathrm{d}x^3}{\mathrm{d}x^2} \\
& \qquad = 6j\,\mathrm{d}x = \frac{\partial^2}{\partial x^2}(x^3) \\
P = x^4\text{:}\ & \frac{P_{j+1}^n - 2P_j^n + P_{j-1}^n}{\mathrm{d}x^2} = \frac{(j+1)^4\,\mathrm{d}x^4 - 2j^4\,\mathrm{d}x^4 + (j-1)^4\,\mathrm{d}x^4}{\mathrm{d}x^2} \\
& \qquad \neq \frac{\partial^2}{\partial x^2}(x^4)
\end{aligned} \tag{1.3.1}$$

Similar considerations apply to the time derivative approximation. The overall accuracy of the scheme per time step is 3rd order. A smaller time step however involves more time steps to reach a given time and because of cumulated errors the total accuracy of the scheme is then only second order. Thus, for example, for calculations up to a specified time, halving the time step will improve accuracy by a factor of four.

The above considerations determine only the rate of convergence of the scheme. The topic of accuracy for variable velocity and different boundary conditions is more involved and beyond the scope of this presentation.

1.4. Stability and numerical dispersion

Assume c = const. and try a travelling wave solution of the form: $P_j^n = \exp \mathrm{i}(kj\,\mathrm{d}x - \omega n\,\mathrm{d}t)$. The spatial derivative approximation yields,

$$\frac{\partial^2 P_j^n}{\partial x^2} \approx \frac{P_{j+1}^n - 2P_j^n + P_{j-1}^n}{\mathrm{d}x^2} \tag{1.4.1}$$

$$= \mathrm{e}^{(-\mathrm{i}\omega n\,\mathrm{d}t)}\,\frac{\mathrm{e}^{\mathrm{i}k(j+1)\,\mathrm{d}x} - 2\,\mathrm{e}^{\mathrm{i}kj\,\mathrm{d}x} + \mathrm{e}^{\mathrm{i}k(j-1)\,\mathrm{d}x}}{\mathrm{d}x^2} \tag{1.4.2}$$

$$= -\frac{4}{\mathrm{d}x^2} \cdot \mathrm{e}^{\mathrm{i}(kj\,\mathrm{d}x - \omega n\,\mathrm{d}t)} \cdot \left[\sin^2 k\,\mathrm{d}x/2\right]$$

Similarly,

$$\frac{\partial^2 P_j^n}{\partial t^2} = \frac{-4}{\mathrm{d}t^2} \cdot \mathrm{e}^{\mathrm{i}(kj\,\mathrm{d}x - \omega n\,\mathrm{d}t)} \cdot \left[\sin^2 \omega\,\mathrm{d}t/2\right]$$

A substitution into (1.2.5) yields,

$$-\frac{1}{c^2\,\mathrm{d}t^2} \sin^2 \omega\,\mathrm{d}t/2 = -\frac{1}{\mathrm{d}x^2} \sin^2 k\,\mathrm{d}x/2$$

or,

$$\sin\left[\omega\,\mathrm{d}t/2\right] = \left[\frac{c\,\mathrm{d}t}{\mathrm{d}x}\right] \sin\frac{k\,\mathrm{d}x}{2}$$

or,

$$\omega = \frac{2}{\mathrm{d}t} \sin^{-1}\left[\frac{c\,\mathrm{d}t}{\mathrm{d}x} \sin\frac{k\,\mathrm{d}x}{2}\right] \tag{1.4.3}$$

This equation which relates $\omega = \omega(k)$ defines a dispersion relation. In a dispersive medium the phase velocity is defined as: $C_p = \omega/k$ and the group velocity as: $U_g = \mathrm{d}\omega/\mathrm{d}k$. Figure 1 plots the normalized phase velocity versus wavenumber for different values of the parameter $\alpha = c\,\mathrm{d}t/\mathrm{d}x < 1$. For stability α must be less or equal to one because otherwise the r.h.s. of (1.4.3) becomes greater than unity for the spatial Nyquist component for which $k\,\mathrm{d}x = \pi$. When $\alpha = 1$ then $C_p = \omega/k = \mathrm{d}x/\mathrm{d}t = c$ and no numerical dispersion exists. When $\alpha < 1$ numerical dispersion is always present.

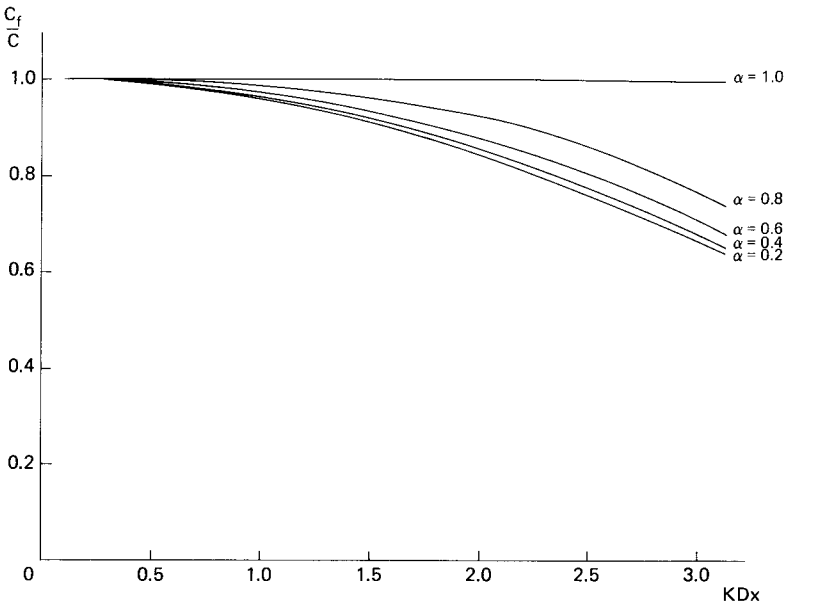

Fig. 1. Normalized phase velocity vs wavenumber for second order differencing scheme.

When the velocity is variable, a different analysis is needed. This analysis can be based on the evaluation of the eigenvalues of the discrete operator $c^2\partial^2/\partial x^2$. However, experience has taught us that for the magnitude of velocity contrasts typically encountered in exploration Geophysics the above results also can be used when c is replaced by the maximum velocity in the grid $c_{\max}$.

For $k\,\mathrm{d}x < \pi/5$ the dispersion is often considered sufficiently small. This value corresponds to a wavelength of 10 grid points.

Example . Determine $\mathrm{d}t$, $\mathrm{d}x$ for a problem of wave propagation in a region with a maximum velocity $C_{\max}$ of 4000 m/sec and a minimum velocity $C_{\min}$ of 1500 m/sec. The desired maximum frequency is 50 Hz.

Answer:

$$\lambda_{\min} = \frac{c_{\min}}{f_{\max}} = \frac{1500}{50} = 30 \text{ m},$$

where $\lambda_{\min}$ is the shortest wavelength present. Therefore, $\mathrm{d}x \approx \lambda_{\min}/10 = 3\text{m}$ and $\mathrm{d}t = \mathrm{d}x/c_{\max} = 3/4000 \approx 0.75\text{msec}$.

1.5. Improving spatial accuracy with higher order schemes

With no loss of generality we can evaluate results at $x = 0$. For the second derivative approximation we only examine schemes with odd number of points. We can then write:

$$\frac{\partial^2 P_0}{\partial x^2} \approx \omega_0 P_0 + \omega_1 (P_1 + P_{-1}) + \cdots + \omega_l (P_l + P_{-l}) \tag{1.5.1}$$

where $l + 1$ is the number of weighting coefficients and we have already used a symmetric form which guarantees that $\partial^2 P_0/\partial x^2 = 0$ for $P_0 = x^\alpha$ with odd α. We now require that (1.5.1) be accurate for all polynomials up to order $2l$. We obtain:

$$\begin{aligned}
&\text{for } P_j = 1 \qquad \omega_0 + 2\omega_1 + \omega_2 + \cdots + 2\omega_l = 0 \\
&\text{for } P_j = (j\,\mathrm{d}x)^2 \qquad 2(\omega_1\,\mathrm{d}x^2 + 4\omega_2\,\mathrm{d}x^2 + \cdots + \omega_l l^2\,\mathrm{d}x^2) = 2 \\
&\qquad \cdots \\
&\text{for } P_j^n = (j\,\mathrm{d}x)^{2l} \qquad 2(\omega_1\,\mathrm{d}x^{2l} + \omega_2 2^{2l}\,\mathrm{d}x^{2l} + \cdots + \omega_l l^{2l}\,\mathrm{d}x^{2l}) = 0
\end{aligned} \tag{1.5.2}$$

We have $l + 1$ linear equations for the unknowns: ω_0, ω_1, ..., ω_l. With a redefinition of the unknowns $v_0 = \omega_0$, and $v_i = 2\omega_i$ for $i > 0$ we get:

$$\begin{aligned}
&v_0 + v_1 + v_2 + \cdots + v_l = 0 \\
&\quad v_1 + 4v_2 + \cdots + l^2 v_l = \frac{2}{\mathrm{d}x^2} \\
&\qquad\qquad \cdots \\
&v_1 + 2^{2l} v_2 + \cdots + l^{2l} v_l = 0
\end{aligned} \tag{1.5.3}$$

The system can be written in matrix form:

$$\begin{bmatrix} 1 & 1 & 1 & \dots & 1 \\ 0 & 1 & 4 & \dots & l^2 \\ \vdots & \vdots & \vdots & \vdots\vdots\vdots & \vdots \\ 0 & 1 & 2^{2l} & \dots & l^{2l} \end{bmatrix} \begin{bmatrix} v_0 \\ v_1 \\ \vdots \\ v_l \end{bmatrix} = \begin{bmatrix} 0 \\ 2/\mathrm{d}x^2 \\ \vdots \\ 0 \end{bmatrix} \tag{1.5.4}$$

The matrix in eq. (1.5.4) is known as the Vandermonde matrix (Hamming, 1978). It can be proven that the matrix is non singular and has a closed form inverse. Denoting this inverse by Υ^{-1} we can then write:

$$\begin{bmatrix} v_0 \\ v_1 \\ \vdots \\ v_l \end{bmatrix} = \begin{bmatrix} & \Upsilon^{-1} & \end{bmatrix} \begin{bmatrix} 0 \\ 2/\mathrm{d}x^2 \\ \vdots \\ 0 \end{bmatrix} \tag{1.5.5}$$

This formula allows to obtain the coefficients for finite difference schemes of any order. In the following, rather then use Υ^{-1} we will solve 1.5.3 directly for examples with a small l.

Example 1 . $l = 2$. We get from eq. (1.5.4):

$$\begin{bmatrix} 1 & 1 \\ 0 & 1 \end{bmatrix} \begin{bmatrix} v_0 \\ v_1 \end{bmatrix} = \begin{bmatrix} 0 \\ 2/\mathrm{d}x^2 \end{bmatrix},$$

from which we get $v_1 = 2/\mathrm{d}x^2$, $v_0 = -2/\mathrm{d}x^2$ and therefore $\omega_0 = v_0 = -2/\mathrm{d}x^2$ and $\omega_1 = v_1/2 = 1/\mathrm{d}x^2$. The differencing scheme becomes:

$$\frac{\partial^2 P_0}{\partial x^2} = \frac{1}{\mathrm{d}x^2}(P_{-1} - 2P_0 + P_1)$$

which is the same scheme we used before.

Example 2 . $l = 3$. We get:

$$\begin{aligned}
v_0 + v_1 + v_2 &= 0 \\
v_1 + 4v_2 &= \frac{2}{\mathrm{d}x^2} \\
v_1 + 16v_2 &= 0
\end{aligned}$$

which gives:

$$v_2 = -\frac{1}{6\,\mathrm{d}x^2} \quad \text{and} \quad v_1 = \frac{8}{3\,\mathrm{d}x^2}, \qquad \text{or}$$

$$\omega_2 = -\frac{1}{12\,\mathrm{d}x^2}, \quad \text{and} \quad \omega_1 = \frac{4}{3\,\mathrm{d}x^2},$$

respectively, and

$$v_0 = \omega_0 = -\frac{5}{2\,\mathrm{d}x^2}.$$

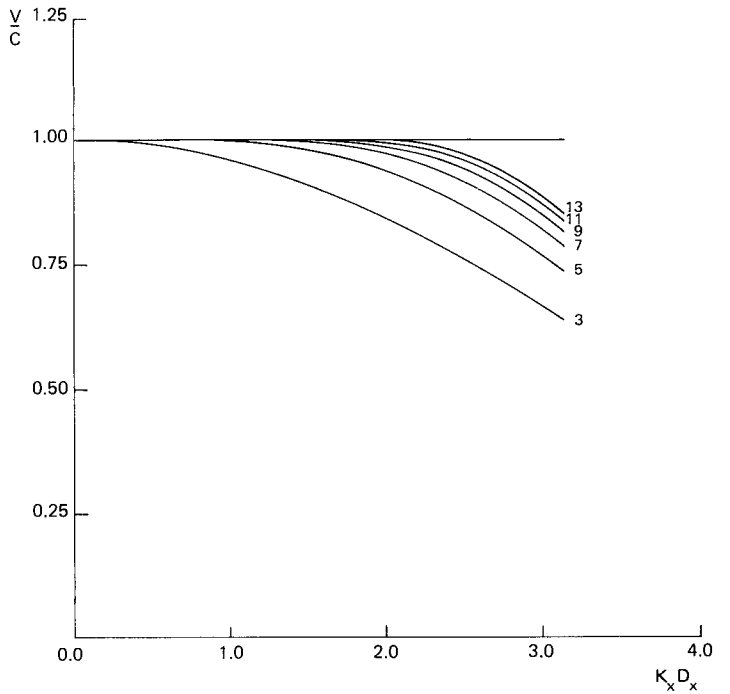

Fig. 2. Phase velocity vs wavenumber for finite-difference schemes of different orders.

The differencing scheme then becomes:

$$\frac{\partial^2 P_0}{\partial x^2} = \frac{1}{\mathrm{d}x^2}\left[-\frac{5}{2}P_0 + \frac{4}{3}(P_1 + P_{-1}) - \frac{1}{12}(P_2 + P_{-2})\right]$$

which is the fourth order differencing scheme.

A fourth order scheme in space and second order in time for solving the acoustic wave equation for constant density then reads:

$$P_j^{n+1} = 2P_j^n - P_j^{n-1} + \frac{c_j^2\,\mathrm{d}t^2}{\mathrm{d}x^2} \times \left[-\frac{5}{2}P_j^n + \frac{4}{3}(P_{j+1}^n + P_{j-1}^n) - \frac{1}{12}(P_{j+2}^n + P_{j-2}^n)\right]. \quad (1.5.6)$$

Higher order finite difference schemes can be derived in the same way.

The question arises of what kind of improvement do higher order schemes bring over the second order scheme which we have studied. The type of numerical dispersion analysis done before could be carried out again yielding phase velocity versus wavenumber plots. Results of this type of analysis are shown in fig. 2. This plot shows that the fourth order scheme brings about a significant improvement over the second order scheme and that the sixth order scheme brings further improvement. However, beyond the sixth order scheme the rate of improvement decreases considerably and it becomes questionable whether the added computational effort with the long derivative operator is worthwhile. Many researchers believe that 4^{th} order or 6^{th} order approximations are optimal.

1.6. Acoustic wave equation with variable density

The acoustic wave equation for variable density in one spatial dimension reads:

$$\frac{\partial}{\partial x}\left(\frac{1}{\rho}\frac{\partial P}{\partial x}\right) = \frac{1}{\rho c^2}\frac{\partial^2 P}{\partial t^2}$$

where ρ is the density (e.g. Kosloff and Baysal, 1982).

We now need a scheme for the spatial derivative term which includes the density. There are many possibilities to achieve this goal but one alternative which also works well in two and three dimensions is to use a two stage approach. Denoting:

$$R_j^n = \frac{\partial}{\partial x}\left(\frac{1}{\rho}\frac{\partial P}{\partial x}\right)_j^n, \quad (1.6.1)$$

the scheme is as follows:

Stage 1: calculate

$$\frac{\partial P_j^n}{\partial x} \approx \frac{P_{j+1}^n - P_{j-1}^n}{2\,\mathrm{d}x},$$

then multiply result by $1/\rho_j$;

Stage 2: calculate

$$R_j^n = \frac{1}{2\,\mathrm{d}x}\left[\frac{1}{\rho_{j+1}}\frac{\partial P_{j+1}^n}{\partial x} - \frac{1}{\rho_{j-1}}\frac{\partial P_{j-1}^n}{\partial x}\right]$$

Stage 3: Perform time integration according to:

$$P_j^{n+1} = 2P_j^n - P_j^{n-1} + \rho_j c_j^2\,\mathrm{d}t^2 R_j^n.$$

It is interesting to compare the accuracy of this scheme with the accuracy of the previous second order scheme for constant density. Assuming constant density $\rho_j = \rho_0$ and velocity $c_j = c_0$ stage 1 can be substituted into stage 2 to yield for R_j^n :

$$\rho_0 R_j^n = \left[\frac{P_{j+2}^n - P_j^n}{2\,\mathrm{d}x} - \frac{P_j^n - P_{j-2}^n}{2\,\mathrm{d}x}\right]\frac{1}{2\,\mathrm{d}x}$$
$$= \frac{1}{4\,\mathrm{d}x^2}\left[P_{j+2}^n - 2P_j^n + P_{j-2}^n\right]. \qquad (1.6.2)$$

This is the same spatial derivative approximation as in the constant density case except that now it corresponds to a grid spacing of $2\,\mathrm{d}x$ instead of $\mathrm{d}x$. This means that the numerical dispersion will occur much earlier (e.g. at longer wavelengths) . This conclusion is not only limited to this case but applies to many other examples where a first derivative approximation is required. The staggered grid approach discussed in the next section offers a solution for achieving equal accuracy with first derivative operators and second derivative operators.

1.7. Staggered grids

The variable density scheme in the previous section can be significantly improved when the first spatial derivatives are calculated between grid points. The stages then run as follows:

Stage 1: calculate

$$\frac{\partial P_{j+1/2}^n}{\partial x} \approx \frac{P_{j+1}^n - P_j^n}{\mathrm{d}x},$$

then multiply result by $1/\rho_{j+1/2}$;

Stage 2: calculate

$$R_j^n = \frac{1}{\mathrm{d}x}\left[\frac{1}{\rho_{j+1/2}}\frac{\partial P_{j+1/2}^n}{\partial x} - \frac{1}{\rho_{j-1/2}}\frac{\partial P_{j-1/2}^n}{\partial x}\right];$$

Stage 3: Perform time integration.

When the density is constant a substitution of stage 1 into stage 2 gives the constant density scheme. Several investigators have suggested using staggered grids in two spatial dimensions for achieving the same type of improvement (Vireaux, 1984, 1986; Levander, 1988). Figure 3 shows an outline for a staggered grid for the acoustic wave equation in two dimensions.

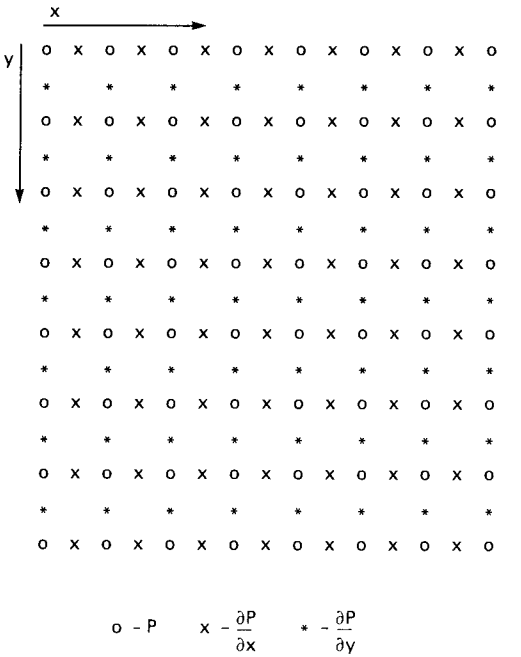

Fig. 3. Staggered grid scheme for acoustic wave equation.

1.8. The Fourier method

The Fourier method attempts to achieve a highly accurate derivative approximation by using the derivative property of the Fourier transform. Given a function $f(x)$ and denoting its Fourier transform by $\tilde{f}(k)$ with k the wavenumber, the derivative property states that the transform of $\partial f/\partial x$ is given by $\mathrm{i}k\tilde{f}(k)$, and likewise, the transform of $\partial^2 f/\partial x^2$ is given by $-k^2\tilde{f}$ (Bracewell, 1978). In the Fourier method $\tilde{f}$ is calculated by the FFT.

For example, given the acoustic wave equation for variable density, the steps of the calculation run as follows:

Stage 1: Calculate $\partial P_j^n/\partial x$:

$$P_j^n \rightarrow \mathrm{FFT} \rightarrow \tilde{P}_\nu^n \rightarrow \mathrm{i}k_\nu \tilde{P}_\nu^n \rightarrow \mathrm{FFT}^{-1} \rightarrow \frac{\partial P_j^n}{\partial x}$$

Multiply the result by $1/\rho_j$ to get $(1/\rho_j)(\partial P_j^n/\partial x)$.

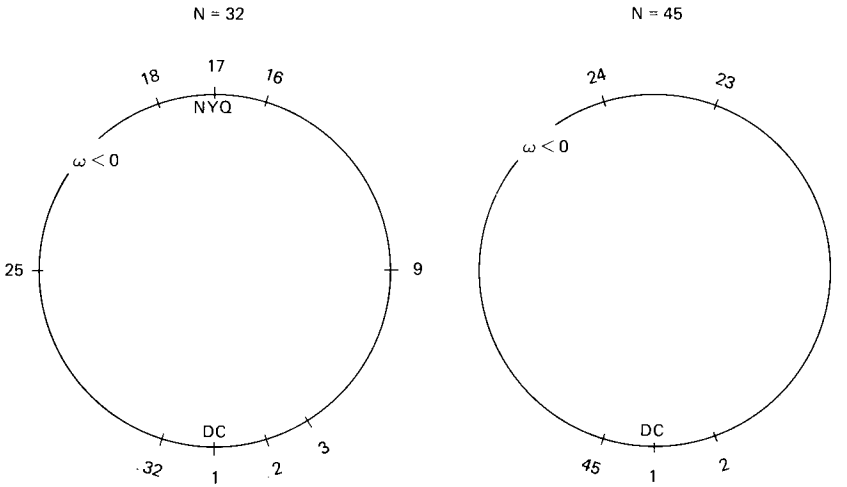

Fig. 4. Circular diagrams for even and odd based FFT's.

Stage 2: Calculate $R_j^n = \frac{\partial}{\partial x}\left(\frac{1}{\rho}\frac{\partial P}{\partial x}\right)_j^n$:

$$\frac{1}{\rho_j}\frac{\partial P_j^n}{\partial x} \rightarrow \text{FFT} \rightarrow \left(\frac{1}{\rho}\widetilde{\frac{\partial P}{\partial x}}\right)_\nu^n \rightarrow \mathrm{i}k_\nu\left(\frac{1}{\rho}\widetilde{\frac{\partial P}{\partial x}}\right)_\nu^n$$
$$\rightarrow \text{FFT}^{-1} \rightarrow \frac{\partial}{\partial x}\left(\frac{1}{\rho}\frac{\partial P}{\partial x}\right)_j^n$$

Stage 3: Perform time integration:

$$P_j^{n+1} = 2P_j^n - P_j^{n-1} + \rho_j c_j^2\,\mathrm{d}t^2 R_j^n$$

Remarks . (a) The method is periodic. For example a wave impinging on the left boundary of the grid will return from the right boundary.
(b) For first derivative approximation it is important to use odd based FFT's. This is because even transforms have a Nyquist component which does not possess the Hermetian property of the derivative (e.g. that a derivative of an even function is odd. and vise versa). The reason for this is as follows: When $f(x)$ is real $\tilde{f}(k)$ is Hermitian (i.e. its even part is real and odd part is imaginary). For the discrete Fourier transform (DFT) k is given by

$$k_\nu = \begin{cases} 2\pi\nu/N\,\mathrm{d}x & \text{for } \nu = 0, 1, \ldots, \frac{N-1}{2} \\ -2\pi(N-\nu)/N\,\mathrm{d}x & \text{for } \nu = \frac{N+1}{2}, \ldots, N-1 \end{cases} \qquad (1.8.1)$$

(for even N, $(N+1)/2$ represents truncation to the closest integer). When N is odd k_ν is an odd function of ν in the periodic sense (e.g. $\tilde{f}(\nu) = -\tilde{f}(-\nu)$ and $\tilde{f}(-\nu) = \tilde{f}(N-\nu)$). Therefore $\mathrm{i}k_\nu\tilde{f}(k_\nu)$ is also Hermitian and $\partial f/\partial x$ becomes real. When N is even k_ν is again odd except for the Nyquist frequency component k_{nyq} for which it is even. Therefore a multiplication by $\mathrm{i}k_{\mathrm{nyq}}\tilde{f}(k_{\mathrm{nyq}})$ will be imaginary-even which would result in an imaginary $\partial f/\partial x$. Consequently, a complete and real derivative operator requires an odd N. Figure 4 shows circular diagram plots which illustrate this point.

1.9. Numerical dispersion and stability

Consider again the constant density acoustic wave equation with constant velocity c and assume a solution of the form $P_j^n = \mathrm{e}^{\mathrm{i}(kj\,\mathrm{d}x - \omega n\,\mathrm{d}t)}$ where k is given by (1.8.1). For the Fourier spatial derivative approximation we get:

$$\frac{\partial^2 P_j^n}{\partial x^2} = -k^2\,\mathrm{e}^{\mathrm{i}(kj\,\mathrm{d}x - \omega n\,\mathrm{d}t)}$$

As with the finite-difference case the temporal approximation will give;

$$\frac{\partial^2 P_j^n}{\partial t^2} = -\frac{4}{\mathrm{d}t^2}\sin^2\frac{\omega\,\mathrm{d}t}{2}\,\mathrm{e}^{\mathrm{i}(kj\,\mathrm{d}x - \omega n\,\mathrm{d}t)}$$

A substitution in the wave equation yields:

$$\frac{2}{c\,\mathrm{d}t}\sin\left(\frac{\omega\,\mathrm{d}t}{2}\right) = k$$

or:

$$\omega = \frac{2}{\mathrm{d}t}\sin^{-1}\left(\frac{kc\,\mathrm{d}t}{2}\right)$$

This equation defines the numerical dispersion relation for the Fourier method. The following conclusions can be drawn:
(a) When $\mathrm{d}t << 1$, $\sin^{-1}(kc\,\mathrm{d}t/2) \approx kc\,\mathrm{d}t/2$ and $\omega/k = c$ meaning practically no dispersion (see fig. 5). Hence unlike with second order finite-differences a decrease in time step size reduces the dispersion. Based on the figure the criterion $\alpha = c\,\mathrm{d}t/\mathrm{d}x < 0.2$ is often used for assuring both stability and small dispersion.
(b) The argument of the inverse sine must be smaller than one. Hence the stability limit $k_{\max}(c\,\mathrm{d}t/2) \leq 1$. As $k_{\max} = \pi/\mathrm{d}x$ therefore $\alpha = (c\,\mathrm{d}t/\mathrm{d}x) < 2/\pi$.

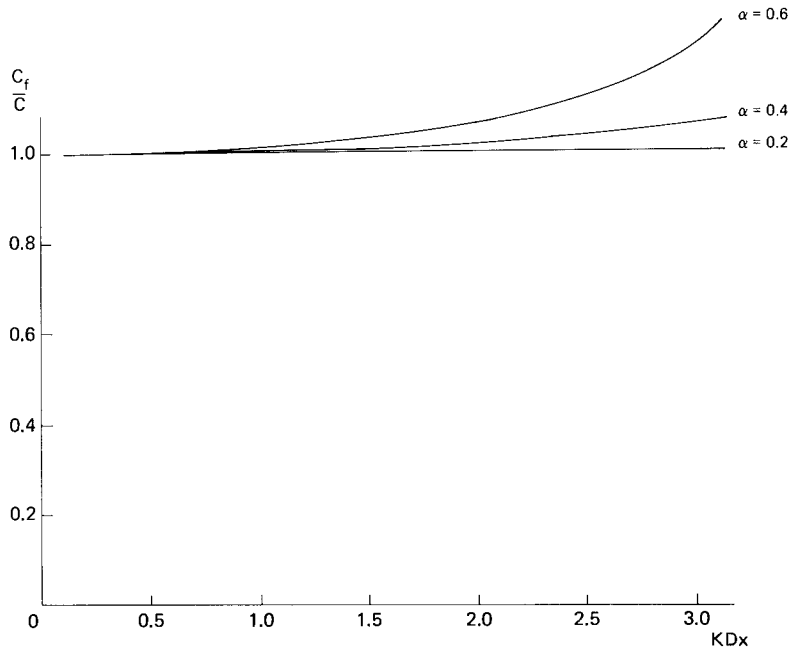

Fig. 5. Phase velocity versus wavenumber for Fourier method.

(c) From the figure it appears that with a sufficiently small dt the numerical dispersion can be avoided. In that case the modeling will be accurate up to the spatial Nyquist frequency which corresponds to a spatial wavelength of two grid points. This is in contrast to the figure of ten grids per wavelength for second order differencing. Though in reality the situation is not quite so ideal, the Fourier method does indeed require much fewer points to achieve the same accuracy as with finite-differences. On the other hand the Fourier method requires more calculation per grid point. It is therefore a subject of debate which method is more economical. The reduction in number of grid points becomes more significant in 2D and 3D.

1.10. Fourier method without FFT

The Fourier method can be applied directly in the space domain by using the convolution property of the Fourier transform. Given two functions $f(x)$ and $g(x)$ we denote their transforms by $\tilde{f}$ and $\tilde{g}$. The convolutional property then states that the transform of the convolution $f * g$ is given by the simple multiplication $\tilde{f}\tilde{g}$ (e.g. Bracewell, 1978). Considering for example the second derivative approximation we can write:

$$\frac{\partial^2 f}{\partial x^2} = \left(-k^2 \tilde{f}\right)^{-1} = \left(-k^2\right)^{-1} * f.$$

When f is discrete the convolution is to be understood in the cyclic sense. $\left(-k^2\right)^{-1}$ denotes the inverse discrete Fourier transform of $-k^2$. It is given by:

$$\left(-k^2\right)_0^{-1} = -\left(\frac{2\pi}{N\,\mathrm{d}x}\right)^2 \frac{L(L+1)}{3} \tag{1.10.1}$$

and

$$\left(-k^2\right)_n^{-1} = \frac{1}{2}\left(\frac{2\pi}{N\,\mathrm{d}x}\right)^2 (-1)^n \frac{\cos\left(\frac{\pi n}{N}\right)}{\sin^2\left(\frac{\pi n}{N}\right)} \quad \text{for } n \neq 0 \tag{1.10.2}$$

with $N = 2L + 1$ (Kosloff and Kessler, 1987). These coefficients can be applied directly to P_j^n as with finite-differences. The result obviously will be the same as with the FFT and it is only a question of economics which method is better. Here however, the derivative operator is extremely long and the usual method of using the FFT is preferable. There exists however a possibility of using shorter smoothed versions of (1.10.1) as spatial domain derivative operators (Mora, 1988). The topic of design of improved derivative operators is discussed later.

1.11. Finite differences using the FFT

The finite-differences derivative approximation consists of a convolution. We can write,

$$\frac{\mathrm{d}^2 f}{\mathrm{d}x^2} = W * f. \tag{1.11.1}$$

For example, with second order finite-differences

$$W = \left(\frac{1}{\mathrm{d}x^2}, \frac{-2}{\mathrm{d}x^2}, \frac{1}{\mathrm{d}x^2}\right),$$

or with fourth order finite-differences

$$W = \left(\frac{-1}{12\,\mathrm{d}x^2}, \frac{4}{3\,\mathrm{d}x^2}, \frac{-5}{2\,\mathrm{d}x^2}, \frac{4}{3\,\mathrm{d}x^2}, \frac{-1}{12\,\mathrm{d}x^2}\right).$$

The coefficients for the second and fourth order finite-difference operator as well as for the Fourier method are plotted in fig. . 6. Using again the convolution property we could calculate the second derivative through the multiplication $\tilde{W}\tilde{f}$ in the spatial frequency domain. For example, for the second order differencing approximation we have seen that $\tilde{W}_\nu = -\frac{4}{\mathrm{d}x^2}\sin^2\frac{k_\nu\,\mathrm{d}x}{2}$, where k_ν is the wavenumber of the FFT. The resulting FD scheme will have periodic boundary conditions.

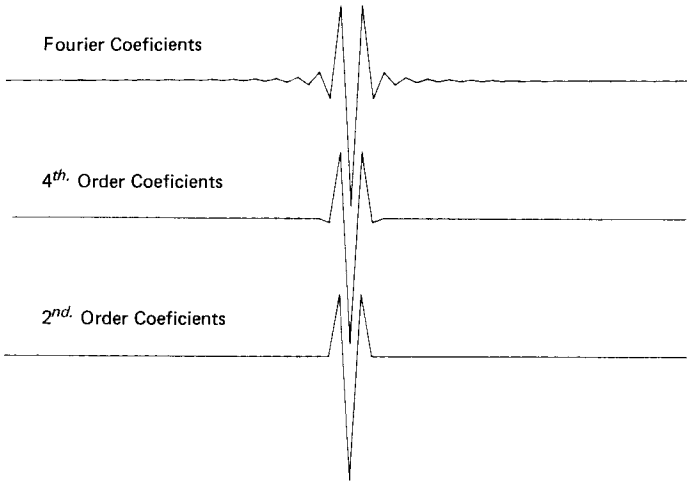

Fig. 6. Operator weights.

This approach, though interesting, is usually less efficient than applying the difference operator directly in the space domain. This is because usually the difference operator is not too long. However the insight gained by the last two alternatives will become useful for the construction of hybrid operators.

1.12. A hybrid method

As shown above the finite-differences derivative operators are accurate for the long wavelengths but fail to give satisfactory results for shorter wavelengths. The use of higher order schemes did not resolve the problem completely. On the other hand the derivative approximation can be recognized as a convolutional operation, and one may seek other linear operators which produce better results.

The convolutional approximation is of the type:

$$\frac{\mathrm{d}^2 f_0}{\mathrm{d}x^2} = \omega_0 f_0 + \omega_1(f_1 + f_{-1}) + \omega_2(f_2 + f_{-2}) + \omega_3(f_3 + f_{-3}) + \cdots + \omega_l(f_l + f_{-l}) \tag{1.12.1}$$

where $\omega_0, \omega_1, \ldots, \omega_l$ need to be determined. This symmetric form assures the correctness of the derivative approximation for odd functions.

We have obtained a successful hybrid scheme by requiring that (1.12.1) be exact for the functions $f = 1$, x^2, x^4 and that it be exact in a least squares sense for the functions $\cos k_\alpha x$, $\alpha = 0 \ldots\ldots M$ with $M > l$. The resulting system reads:

$$\begin{aligned}
\omega_0 + 2\omega_1 \cos k_0 + 2\omega_2 \cos 2k_0 + \cdots + 2\omega_l \cos lk_0 &= -k_0^2 \\
\omega_1 + 2\omega_1 \cos k_1 + 2\omega_2 \cos 2k_1 + \cdots + 2\omega_l \cos lk_1 &= -k_1^2 \\
&\cdots \\
\omega_M + 2\omega_M \cos k_M + 2\omega_2 \cos 2k_M + \ldots + 2\omega_l \cos lk_M &= -k_M^2,
\end{aligned}$$

with $0 < k_\alpha < \pi/\,\mathrm{d}x$. The correctness for $f = 1, x^2, x^4$ etc. was introduced through Lagrange multipliers. The constraints are given by:

$$\begin{aligned}
\omega_0 + 2\omega_1 + \cdots + 2\omega_l &= 0 \\
2\omega_1 + 8\omega_2 + \cdots + 2l^2\omega_l &= 2 \\
&\vdots
\end{aligned}$$

Attempts to get weights for the first derivative approximation were much less successful unless one uses staggered schemes in which first derivatives are calculated between grid points.

A second alternative for obtaining the coefficients of a derivative approximation is to retain the first few terms of a smoothed second derivative of a spike based on the Fourier method (Mora, 1988).

1.13. The finite-element method

Unlike the methods which we have already discussed, the finite-element technique originates from an integral statement which can either be a variational principle or a Galerkin method. The end result is again a convolutional spatial operator which in many cases can be shown to be equivalent to operators obtained by finite-differences. In the following we outline the finite-element method and show the equivalence between finite-elements and finite-differences in 1 dimension.

1.13.1. Notation and spatial discretization

With the finite-element method the variables are evaluated by interpolation from nodal values. We consider a second order isoparametric method (e.g. Zienkiewitcz, 1977). The interpolation can be written as:

$$p(x_i) = \{\boldsymbol{\Phi}(\boldsymbol{x}_i)\}^T \{\boldsymbol{P}\}, \quad i = 1, \ldots, D, \tag{1.13.1}$$

where D is the number of spatial dimensions, $\{\boldsymbol{P}\}$ is a column vector of the values of $p(x_i)$ at the nodes, and $\{\boldsymbol{\Phi}\}^T$ is a row vector of spatial interpolation functions. For example in one spatial dimension:

$$\{\Phi\}_n = \begin{cases} \dfrac{x - x_{n-1}}{x_n - x_{n-1}} & \text{for } x_{n-1} \le x \le x_n \\ \dfrac{x_{n+1} - x}{x_{n+1} - x_n} & \text{for } x_n \le x \le x_{n+1} \\ 0 & \text{otherwise.} \end{cases} \tag{1.13.2}$$

Rather than calculate the interpolation functions directly as in (1.13.2), it is easier, in particular in two or three dimensions, to map each element into a simplified coordinate system which we term the Z system. Each element has its individual mapping and local numbering scheme according to the convention in fig. 7. The interpolation functions within an element in this new coordinate system are given by:

$$\phi_n(z_i) = \frac{1}{2^D} \prod_{i=1}^{D} (1 + z_i Z_i^n), \quad n = 1, \ldots, 2^D, \tag{1.13.3}$$

where $Z_i^n = \pm 1$ (fig. 7), and the interpolation reads

$$P(Z_i) = \sum_{i=1}^{2^D} \phi_n(Z_i) P_n, \tag{1.13.4}$$

where P_n is the pressure at the n^{th} node surrounding the element. For example, in two dimensions,

$$\begin{cases} Z_1^1 = -1 & Z_1^2 = 1 & Z_1^3 = -1 & Z_1^4 = 1 \\ Z_2^1 = -1 & Z_2^2 = -1 & Z_2^3 = 1 & Z_2^4 = 1 \end{cases}$$

In one dimension the interpolation reads:

$$p(z_1) = \frac{1}{2}(1 - z_1)P^1 + \frac{1}{2}(1 + z_1)P^2,$$

and it can be seen that the interpolation requirements $p(z_1 = Z_1^1) = P^1$, and $p(z_1 = Z_1^2) = P^2$ are satisfied.

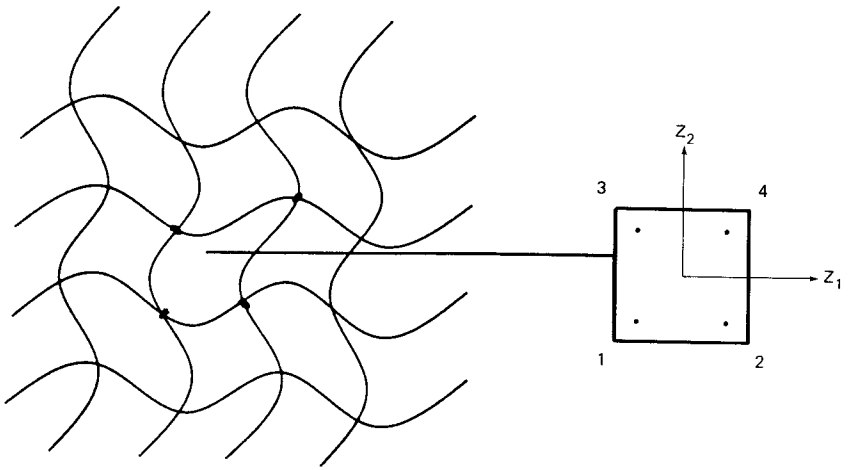

Fig. 7. Finite-element mapping scheme.

In two dimensions the interpolation reads:

$$\begin{aligned} p(z_1, z_2) &= \sum_{i=1}^{4} \phi_i(z_1, z_2) P^i \\ &= \frac{1}{4} \left[(1 - z_1)(1 - z_2)P^1 + (1 + z_1)(1 - z_2)P^2 \right. \\ &\quad \left. + (1 - z_1)(1 + z_2)P^3 + (1 + z_1)(1 + z_2)P^4 \right] \end{aligned} \tag{1.13.5}$$

The local interpolation functions are also used for the mapping between the global X system and the local Z system with an element. Particularly,

$$x_i(z_k) = \sum_{n=1}^{2^D} \phi_n(z_k) X_i^n, \tag{1.13.6}$$

where X_i^n are the coordinates of the nodes of the element under consideration. By differentiation of (1.13.4) and (1.13.6) we also get:

$$\frac{\partial p}{\partial z_m} = \sum_{n=1}^{2^D} \frac{\partial \phi_n(z_k)}{\partial z_m} P^n \tag{1.13.7}$$

and,

$$\frac{\partial x_i}{\partial z_m} = \sum_{n=1}^{2^D} \frac{\partial \phi_n(z_k)}{\partial z_m} X_i^n. \tag{1.13.8}$$

The entries of $\partial x_i/\partial z_m$ allow the calculation of $\partial z_q/\partial x_l$ by a matrix inversion. The values of $\partial p/\partial x_i$ within each element can now be evaluated by the chain rule:

$$\frac{\partial p}{\partial x_i}(x_k) = \frac{\partial p}{\partial z_l}\frac{\partial z_l}{\partial x_i}, \tag{1.13.9}$$

where a repeated index implies summation over the number of spatial dimensions. We now have all the tools for evaluating quantities within a given element. When passing to a different element a new mapping and local coordinate system are used.

1.13.2. Variational principle

We consider the acoustic wave equation with variable density:

$$\frac{\partial}{\partial x_i}\left(\frac{1}{\rho}\frac{\partial p}{\partial x_i}\right) = \frac{1}{\rho c^2}\ddot{p} + s. \tag{1.13.10}$$

Again repeated indices imply summation over the number of spatial dimensions. We are interested in the solution within a volume V bounded by a surface S (in 2D we actually mean within an area bounded by a line). The latter is divided into S_p, the portion on which pressure boundary conditions are specified, and S_{dp}, the portion on which normal accelerations are given (or pressure flux).

We consider a small pressure variation δp which is consistent with all boundary conditions, and therefore vanishes on S_p. The variational principle equivalent to (1.13.10) is obtained by premultiplying it by δp and integrating over the volume V. An application of Gauss's theorem then yields:

$$-\int_V \frac{1}{\rho}\frac{\partial \delta p}{\partial x_i}\frac{\partial p}{\partial x_i}\,\mathrm{d}V = \int_V \delta p \frac{1}{\rho c^2}\ddot{p}\,\mathrm{d}V + \int_V \delta p s\,\mathrm{d}V - \int_{S_{dp}} \delta p \frac{1}{\rho}\frac{\partial p}{\partial x_i} n_i\,\mathrm{d}S, \tag{1.13.11}$$

where $\boldsymbol{n}$ is the normal to the surface S. The numerical approximation to (1.13.11) is obtained by considering only variations δp according to the interpolation (1.13.1),

$$\delta p = \{\boldsymbol{\Phi}\}^T \{\delta \boldsymbol{P}\} = \{\delta \boldsymbol{P}\}^T \{\boldsymbol{\Phi}\}.$$

Substitution into (1.13.11) yields,

$$\{\delta \boldsymbol{P}\}^T \left[\int_V \frac{1}{\rho}\frac{\partial}{\partial x_i}\{\boldsymbol{\Phi}\}\frac{\partial p}{\partial x_i}\,\mathrm{d}V + \int_V \frac{1}{\rho c^2}\{\boldsymbol{\Phi}\}\ddot{p}\,\mathrm{d}V + \int_V \{\boldsymbol{\Phi}\} S\,\mathrm{d}V - \int_{S_{dp}} \frac{1}{\rho}\frac{\partial p}{\partial x_i} n_i\,\mathrm{d}S\right] = 0 \tag{1.13.12}$$

Since $\{\delta \boldsymbol{P}\}$ is arbitrary, the expression within the square brackets must be identically zero. Expressing $\partial p/\partial x_i$ and $\ddot{p}$ by the interpolation according to (1.13.9), (1.13.5), (1.13.6) and (1.13.1) respectively gives a set of ordinary differential equations for the nodal pressures $\{\boldsymbol{P}\}$:

$$\boldsymbol{K}\{\boldsymbol{P}(t)\} + \boldsymbol{M}\left\{\ddot{\boldsymbol{P}}\right\} + \{\boldsymbol{S}\} = 0, \tag{1.13.13}$$

where $\boldsymbol{K}$ the stiffness matrix, $\boldsymbol{M}$ the mass matrix, and $\{\boldsymbol{S}\}$ the generalized source are respectively given by,

$$\boldsymbol{K} = \int_V \frac{1}{\rho}\frac{\partial\{\boldsymbol{\Phi}\}}{\partial x_i}\frac{\partial\{\boldsymbol{\Phi}\}^T}{\partial x_i}\,\mathrm{d}V \tag{1.13.14}$$

$$\boldsymbol{M} = \int_V \frac{1}{\rho c^2}\{\boldsymbol{\Phi}\}\{\boldsymbol{\Phi}\}^T\,\mathrm{d}V, \tag{1.13.15}$$

$$\{\boldsymbol{S}\} = \int_V \{\boldsymbol{\Phi}\} s\,\mathrm{d}V - \int_{S_{dp}} \{\boldsymbol{\Phi}\}\frac{1}{\rho}\frac{\partial p}{\partial x_i} n_i\,\mathrm{d}S. \tag{1.13.16}$$

The integrals in eqs. (1.13.14)–(1.13.16) can be evaluated numerically. The volume integrals are carried out element by element each time using the local Z system according to the principle:

$$\int_V [\cdot]\,\mathrm{d}V = \sum_{\text{elements}} \int_{V_e} [\cdot] J\,\mathrm{d}z_1 \ldots \mathrm{d}z_D,$$

where $[\cdot]$ denotes the quantity to be integrated and J is the Jacobian $|\partial x_l/\partial z_q|$. The integrations can conveniently be evaluated by second order Gaussian quadrature. In actual calculations the mass matrix $\boldsymbol{M}$ is often replaced by the diagonal lumped mass matrix $\vec{\boldsymbol{M}}$ in which each entry is equal to the sum of all entries in the same row of $\boldsymbol{M}$. With this matrix, equation (1.13.13) can be rewritten as:

$$\left\{\ddot{\boldsymbol{P}}\right\} = -\vec{\boldsymbol{M}}^{-1}\left[\boldsymbol{K}\{\boldsymbol{P}(t)\} + \{\boldsymbol{S}(t)\}\right]. \tag{1.13.17}$$

This equation can be integrated by standard techniques such as second order temporal differencing. The source vector $\{\boldsymbol{S}(t)\}$ is assumed known while the solution yields the nodal pressures $\{\boldsymbol{P}(t)\}$.

1.13.3. Remarks

(a) The stiffness matrix in one dimension

We consider wave propagation in a medium with uniform properties ρ_0, c_0 and a discretization on a uniform grid with spacing $\mathrm{d}x$. Considering a particular element e we get by (1.13.3):

$$\begin{cases} \phi_1(z_1) = \dfrac{1 - z_1}{2} \\ \phi_2(z_1) = \dfrac{1 + z_1}{2}. \end{cases}$$

also,

$$\begin{cases} \dfrac{\partial \phi_1}{\partial z_1} = -\dfrac{1}{2} \\ \dfrac{\partial \phi_2}{\partial z_1} = \dfrac{1}{2}. \end{cases}$$

Since

$$\frac{\partial}{\partial x} = \frac{\partial z_1}{\partial x}\frac{\partial}{\partial z_1} = \frac{2}{\mathrm{d}x}\frac{\partial}{\partial z_1}$$

then,

$$\begin{cases} \dfrac{\partial \phi_1}{\partial x} = -\dfrac{1}{\mathrm{d}x} \\ \dfrac{\partial \phi_2}{\partial x} = \dfrac{1}{\mathrm{d}x}. \end{cases}$$

Since $\boldsymbol{K} = \sum_{\text{elements}} \boldsymbol{K}^e$, the contribution $\boldsymbol{K}^e$ to $\boldsymbol{K}$ in the local numbering system becomes:

$$\boldsymbol{K}^e_{11} = \boldsymbol{K}^e_{22} = \int_{V_e} \frac{\partial \phi_1}{\partial x}\frac{\partial \phi_1}{\partial x}\frac{1}{\rho_0}\,\mathrm{d}x = \frac{1}{\rho_0\,\mathrm{d}x},$$

and,

$$\boldsymbol{K}^e_{12} = \boldsymbol{K}^e_{21} = \int_{V_e} \frac{\partial \phi_1}{\partial x}\frac{\partial \phi_2}{\partial x}\frac{1}{\rho_0}\,\mathrm{d}x = -\frac{1}{\rho_0\,\mathrm{d}x},$$

when the stiffness matrix is summed, $\boldsymbol{K}^e_{11}$ and $\boldsymbol{K}^e_{22}$ contribute to the diagonal entries of $\boldsymbol{K}$ while $\boldsymbol{K}^e_{12}$ and $\boldsymbol{K}^e_{21}$ contribute to the entries above and below the diagonal respectively. The stiffness matrix is then given by:

$$\boldsymbol{K} = -\frac{1}{\rho_0\,\mathrm{d}x}\begin{pmatrix} \cdots & \cdots & \cdots & & & & \\ 1 & -2 & 1 & & & & \\ & 1 & -2 & 1 & & & \\ & & 1 & -2 & 1 & & \\ & & & \ddots & \ddots & \ddots & \\ & & & & 1 & -2 & 1 \\ & & & & \cdots & \cdots & \cdots \end{pmatrix}$$

The first and last rows are determined by the boundary conditions. This matrix can be identified as the second order differencing operator multiplied by $-\mathrm{d}x/\rho_0$. Finite elements and second order differencing are therefore identical. When the parameters ρ and c are variable it can be shown that the stiffness matrix is equivalent to the staggered finite-difference scheme of section (1.7).

(b) Alternative Formulation Of $\boldsymbol{K}\{\boldsymbol{P}\}$

It is sometimes more economical not store the stiffness matrix but rather evaluate $K\{\boldsymbol{P}\}$ implicitly. By (1.13.12) and (1.13.14) we see that:

$$\{\boldsymbol{R}\} = \boldsymbol{K}\{\boldsymbol{P}\} = \sum_{\text{elements}} \int_{V_e} \frac{1}{\rho}\frac{\partial}{\partial x_i}\{\boldsymbol{\Phi}\}\frac{\partial p}{\partial x_i}\,\mathrm{d}V \tag{1.13.18}$$

Given a nodal vector $\{\boldsymbol{P}\}$ the evaluation runs as follows:

(1) For a given element e evaluate

$$\frac{\partial p}{\partial x_i} = \frac{\partial p}{\partial z_l}\frac{\partial z_l}{\partial x_i}$$

at the quadrature points.

(2) Multiply the results by

$$\frac{1}{\rho}\frac{\partial}{\partial x_i}\{\boldsymbol{\Phi}\} = \frac{1}{\rho}\frac{\partial}{\partial z_l}\{\boldsymbol{\Phi}\}\frac{\partial z_l}{\partial x_i}$$

at the quadrature points. Only the entries of $\{\boldsymbol{\Phi}\}$ which correspond to nodes surrounding the element e need to be considered because all others are zero.

(3) Perform integration according to:

$$\int_{V_e} \frac{1}{\rho}\frac{\partial}{\partial x_i}\{\boldsymbol{\Phi}\}\frac{\partial p}{\partial x_i}\,\mathrm{d}V = \sum_{quad}\frac{1}{\rho}\frac{\partial}{\partial x_i}\{\boldsymbol{\Phi}\}\frac{\partial p}{\partial x_i}J\cdot 2^D\,,$$

where two point quadrature is assumed (with weights of unity).

(4) Cumulate values of $\{\boldsymbol{R}\}$ for the entries corresponding to the nodes surrounding the element e.

(c) Evaluation of $\boldsymbol{K}\{\boldsymbol{P}\}$ in 2D using one point quadrature

Paradoxically using a one quadrature point at the center of the element instead of four (e.g. using the trapezoidal rule of integration) can improve results in certain situations once provision is given for hourglass modes (Kosloff and Frazier, 1977). Obviously when the stiffness matrix is not stored this results in a large savings in computer time. Interestingly, it can be shown that for a uniform square grid one quadrature integration yields an operator which is equivalent to a finite-difference staggered scheme. For example

$$\int_{V_e}\frac{\partial}{\partial x_1}\{\boldsymbol{\Phi}\}\frac{1}{\rho}\frac{\partial p}{\partial x_1}\,\mathrm{d}V$$

is identical to within a constant to the differencing scheme:

(1) Calculate at the element centers,

$$\frac{\partial p}{\partial x_1}_{i+1/2\ j+1/2} = \frac{1}{2\,\mathrm{d}x}\left(P_{i+1\ j+1}+P_{i+1\ j}-P_{i\ j+1}-P_{i\ j}\right)$$

(2) Multiply the result by $1/\rho_{i+1/2j+1/2}$.

(3) Calculate at the nodes.

$$\frac{\partial}{\partial x_1}\left(\frac{1}{\rho}\frac{\partial p}{\partial x_1}\right)_{ij} = \frac{1}{2\,\mathrm{d}x}\left(P_{i+1/2j+1/2}+P_{i+1/2j-1/2}-P_{i-1/2j+1/2}-P_{i-1/2j-1/2}\right)$$

Similarly

$$\int_{V_e}\frac{\partial}{\partial x_2}\{\boldsymbol{\Phi}\}\frac{1}{\rho}\frac{\partial p}{\partial x_2}\,\mathrm{d}V$$

can be shown to be equivalent to

$$\frac{\partial}{\partial x_2}\left(\frac{1}{\rho}\frac{\partial p}{\partial x_2}\right)$$

by differencing.

In conclusion although finite-element appears at first different from finite-differences, a closer look shows that the methods are very similar at least for the situations encountered in modeling wave propagation in the Earth. The main advantage of finite-elements is the flexibility in handling boundary conditions and irregular structures. These advantages are less important in exploration Geophysics. Experience has shown that it is extremely difficult to come up with good grid generators to grid around complicated structures and heterogeneities. It is therefore still advantageous to use "stair stepping" as with finite-differences and the Fourier method. Economically finite- elements are usually slower or at least not faster than finite differences.

The above formulation was for a second order spatial scheme. The extension to higher order schemes for dynamic codes is not trivial because of the lumping of the mass matrix which may reduce the accuracy.

2. Two dimensional and three dimensional acoustic forward modeling by the Fourier method

2.1. The multi dimensional acoustic wave equation and the Fourier solution method

The main concepts of 2D and 3D Fourier method solutions of the acoustic wave equation are not very different from those of the 1D solution previously introduced. The point of departure is the acoustic wave equation which in two dimensions reads,

$$\frac{\partial}{\partial x}\left(\frac{1}{\rho}\frac{\partial P}{\partial x}\right)+\frac{\partial}{\partial y}\left(\frac{1}{\rho}\frac{\partial P}{\partial y}\right)=\frac{1}{\rho c^2}\ddot{P}+S \qquad (2.1.1)$$

where x and y are respectively the horizontal and vertical coordinates. In three dimensions the equation reads,

$$\frac{\partial}{\partial x}\left(\frac{1}{\rho}\frac{\partial P}{\partial x}\right)+\frac{\partial}{\partial y}\left(\frac{1}{\rho}\frac{\partial P}{\partial y}\right)+\frac{\partial}{\partial z}\left(\frac{1}{\rho}\frac{\partial P}{\partial z}\right)=\frac{1}{\rho c^2}\ddot{P}+S \qquad (2.1.2)$$

where now z denotes the vertical coordinate. As in the 1D case the Fourier method includes both temporal and spatial discretizations. For example in three dimensions $P^n(i,j,k)=P(x=i\,\mathrm{d}x, y=j\,\mathrm{d}y, z=k\,\mathrm{d}z, t=n\,\mathrm{d}t)$, and:

$$R^n(i,j,k)=\left(\frac{\partial}{\partial x}\left(\frac{1}{\rho}\frac{\partial}{\partial x}\right)+\frac{\partial}{\partial y}\left(\frac{1}{\rho}\frac{\partial}{\partial y}\right)+\frac{\partial}{\partial z}\left(\frac{1}{\rho}\frac{\partial}{\partial z}\right)\right)P^n, \qquad (2.1.3)$$

and,

$$S^n(i,j,k) = S(x = i\,\mathrm{d}x, y = j\,\mathrm{d}y, z = k\,\mathrm{d}z, t = n\,\mathrm{d}t).$$

The derivative terms in R^n are calculated using FFT's along lines in the x, y, and z directions. First $(\partial/\partial x)\left(\frac{1}{\rho}\frac{\partial}{\partial x}\right)$ is calculated along x lines, then $\frac{\partial}{\partial y}\left(\frac{1}{\rho}\frac{\partial}{\partial y}\right)$ and $\frac{\partial}{\partial z}\left(\frac{1}{\rho}\frac{\partial}{\partial z}\right)$ are calculated along y lines and z lines respectively. Time integration is carried out again by temporal differencing according to:

$$\begin{aligned} P^{n+1}(i,j,k) =& 2P^n(i,j,k) - P^{n-1}(i,j,k) + c^2\rho\,\mathrm{d}t^2\,(R^n(i,j,k) \\ & - S^n(i,j,k)) \end{aligned}$$

2.2. Stability and numerical dispersion

Assuming constant ρ and c with no source term we try a solution:
$P^n(l,j) = \exp[\mathrm{i}(k_x l\,\mathrm{d}x + k_y j\,\mathrm{d}y - \omega n\,\mathrm{d}t)]$, for two dimensional propagation.

A substitution in (2.1.1) yields,

$$\begin{aligned} &\frac{\partial}{\partial x}\left(\frac{1}{\rho}\frac{\partial P^n}{\partial x}\right) + \frac{\partial}{\partial y}\left(\frac{1}{\rho}\frac{\partial P^n}{\partial y}\right) = \\ &\quad -\frac{1}{\rho}\left(k_x^2 + k_y^2\right)\exp[\mathrm{i}(k_x l\,\mathrm{d}x + k_y j\,\mathrm{d}y - \omega n\,\mathrm{d}t)] \end{aligned} \tag{2.2.1}$$

and,

$$\frac{\partial^2 P^n}{\partial t^2} = -\frac{4}{\mathrm{d}t^2}\sin^2\frac{\omega\,\mathrm{d}t}{2}\exp[\mathrm{i}(k_x l\,\mathrm{d}x + k_y j\,\mathrm{d}y - \omega n\,\mathrm{d}t)],$$

Together these equations give the dispersion relation,

$$\sqrt{k_x^2 + k_y^2} = \frac{2}{c\,\mathrm{d}t}\sin\frac{\omega\,\mathrm{d}t}{2}$$

An important feature is that the dispersion is isotropic (unlike with many finite-difference schemes). The stability region is defined by

$$\sqrt{k_x^2 + k_y^2}\cdot\frac{c\,\mathrm{d}t}{2} < 1$$

The stability limit is for $k_x^{\max} = \pi/\mathrm{d}x$ and $k_y^{\max} = \pi/\mathrm{d}y$. Therefore

$$\left(\frac{1}{\mathrm{d}x^2} + \frac{1}{\mathrm{d}y^2}\right)^{\frac{1}{2}}\cdot c\,\mathrm{d}t < \frac{2}{\pi}$$

For $\mathrm{d}x = \mathrm{d}y$ the stable region is $\alpha = c\,\mathrm{d}t/\mathrm{d}x < \sqrt{2}/\pi$ as compared to $2/\pi$ for 1D. A similar analysis for 3D would give $2\sqrt{3}/3\pi$.

2.3. Problem design

For illustration we present the main steps in preparing a numerical simulation for a typical problem in exploration geophysics. The steps run as follows:

1. Determine the size of the region to be modeled (e.g. 5 Km * 3 Km), the maximum and minimum velocities in the region (for example 4000 m/s and 2000 m/s) and the highest frequency $f_{\max}$ which will be needed (e.g. 50 Hz). Determine the final time needed (e.g. 3 sec).
2. Calculate the grid size by $\mathrm{d}x = \lambda_{\min}/2 = c_{\min}/2f_{\max}$ (here $2000/(2\cdot 50) = 20\mathrm{m}$) where $\lambda_{\min}$ is the shortest wave which can be propagated without aliasing.
3. Use $c_{\max}$ to determine the time step size according to $c_{\max}\,\mathrm{d}t/\mathrm{d}x < 0.2$ (here $\mathrm{d}t < 0.2\cdot 20/4000 = 1\cdot 10^{-3}$ sec).
4. Run the problem for the required number of time steps $t_{\max}/\mathrm{d}t$.

The source time history should be chosen as a band limited wavelet (e.g. a Ricker wavelet). The results of calculations are usually given in the form of snapshots at selected times and time sections along selected lines in the grid.

2.4. Different types of wave equations

Depending on the application there are a number of different wave equations which can be used for acoustic modeling. These include the variable density wave equation, the constant density wave equation, the nonreflecting wave equation and the one way wave equation of Gazdag (1981).

The variable density wave equation for two and three dimensions is given by (2.1.1) and (2.1.2) respectively. When the density ρ in (2.1.1) or (2.1.2) is constant one obtains the constant density wave equations given by,

$$\frac{\partial^2 P}{\partial x^2} + \frac{\partial^2 P}{\partial y^2} = \frac{1}{c^2}\frac{\partial^2 P}{\partial t^2} \tag{2.4.1}$$

or in three dimensions.

$$\frac{\partial^2 P}{\partial x^2} + \frac{\partial^2 P}{\partial y^2} + \frac{\partial^2 P}{\partial z^2} = \frac{1}{c^2}\frac{\partial^2 P}{\partial t^2}. \tag{2.4.2}$$

In actual applications equations (2.1.1) and (2.4.1) (or (2.1.2) and (2.4.2) in 3D) give identical travel times and critical reflection angles. The solutions will differ however in amplitude values when the density is variable. The non reflecting wave equation can be derived from (2.1.1) or (2.1.2) by assuming constant impedance $\rho c = \alpha$. The resulting equation in 2D is given by:

$$\frac{\partial}{\partial x}\left(c\frac{\partial P}{\partial x}\right) + \frac{\partial}{\partial y}\left(c\frac{\partial P}{\partial y}\right) = \frac{1}{c}\frac{\partial^2 P}{\partial t^2} \tag{2.4.3}$$

With this equation very little energy is reflected from a velocity contrast (for normal incidence the reflection coefficient is zero) (Baysal et al., 1984). The equation is useful for normal incidence modeling where it is desirable to avoid multiple reflections.

Finally the one wave equation in 2D (Gazdag, 1981) is given by:

$$\left(\frac{\partial^2}{\partial x^2} + \frac{\partial^2}{\partial y^2}\right)^{1/2} P = \frac{1}{c}\frac{\partial P}{\partial t}$$

where the square root derivative operator is to be understood in the sense,

$$\left(\frac{\partial^2}{\partial x^2} + \frac{\partial^2}{\partial y^2}\right)^{1/2} \rightarrow \mathrm{i}\,\mathrm{sgn}\,k_y \left(k_x^2 + k_y^2\right)^{1/2}$$

This equation allows energy to propagate only upward (or downward depending on the sign choice). Like the nonreflecting wave equation it is useful for normal incidence modeling.

2.5. *Exploding reflector concept*

A zero offset seismic section (or CDP stacked section) is a result of many experiments (shots), and therefore would seem to require many runs to produce. The exploding reflector concept allows to obtain a section which approximates a zero offset section in one single run.

A source proportional to the reflection coefficients is placed on the interfaces and is initiated at time zero. All the velocities for the calculation must be halved in order to get correct arrival times.

2.6. *Free surface*

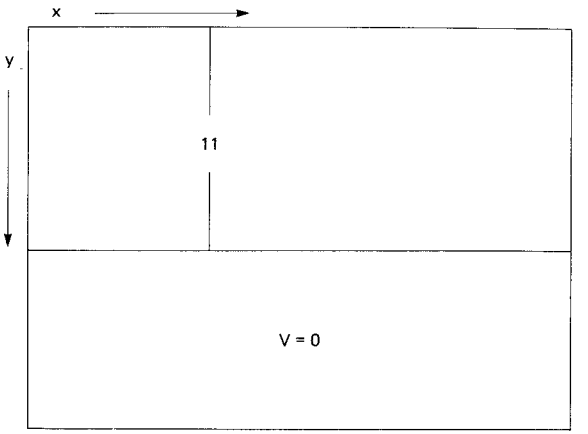

Fig. 8. Free surface implementation for Fourier method.

The free surface boundary condition on the Earth's surface ($P = 0$ at $y = 0$ for 2D) appears at first difficult to achieve with the Fourier method which is periodic in all directions. However, we found that by including a wide zone above the mesh (or below because of periodicity) with zero velocity (fig. 8), this boundary condition can be effected with very high accuracy (in the acoustic case). The width of the zone should be about the same as the region of interest (e.g. FFT's in the vertical dimension are doubled in length). Computationaly the data need not be stored in region l_2. Horizontal derivatives need to be calculated only in region l_1. For the vertical derivatives l_2 zeros are added to the pressure before calculation of the derivatives. For the variable density case (or nonreflecting equation) the value of the density in the region l_2 is taken to be equal to the value at the surface ($y = 0$).

2.7. *Absorbing boundary conditions*

In order to approximate the Earth correctly, it is important to eliminate reflections or wraparound from the boundaries of the mesh. For finite-differences Clayton and Enquist (1977) have shown that a one way wave equation could be used along the boundaries of the mesh, thus preventing energy from reflecting back into the grid. However, for the Fourier method which is periodic and global it is not clear that such a procedure would work.

A different approach was suggested by Cerjan et al. (1985), and Kosloff and Kosloff (1986). This method includes an absorbing strip along the boundaries of the numerical mesh. At the end of each time step the values

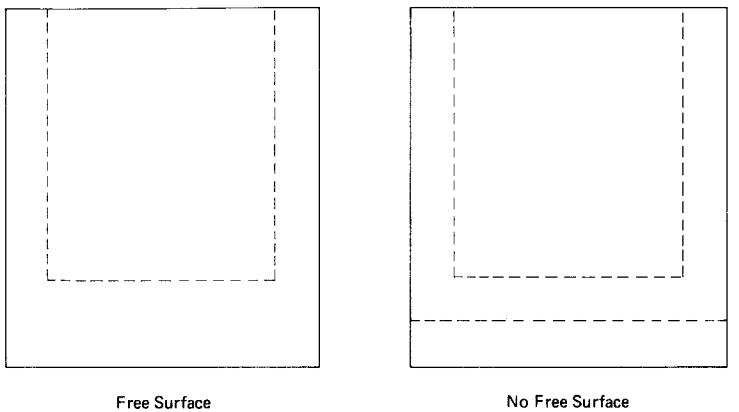

Fig. 9. Absorbing regions.

of P^n and P^{n-1} in the strip are multiplied by a reduction factor which is slightly less than one (usually the values are about 0.92 on the boundaries and increase slowly to 1). The width of the strip is on the order of fifteen grid points (fig. 9).

This approach can be justified on more solid grounds as follows (Kosloff and Kosloff, 1986). Considering for example the variable density acoustic wave equation (2.1.1), it can be written as a system of coupled equations according to,

$$\frac{\partial}{\partial t}\begin{bmatrix} P \\ V \end{bmatrix} = \begin{bmatrix} 0 & 1 \\ A & 0 \end{bmatrix}\begin{bmatrix} P \\ V \end{bmatrix} + \begin{bmatrix} 0 \\ S' \end{bmatrix} \tag{2.7.1}$$

where

$$S' = \rho c^2 S \quad \text{and}$$
$$A = \rho c^2 \left(\frac{\partial}{\partial x}\left(\frac{1}{\rho}\frac{\partial}{\partial x}\right) + \frac{\partial}{\partial y}\left(\frac{1}{\rho}\frac{\partial}{\partial y}\right)\right)$$

An absorbing system then becomes,

$$\frac{\partial}{\partial t}\begin{bmatrix} P \\ V \end{bmatrix} = \begin{bmatrix} -\gamma & 1 \\ A & -\gamma \end{bmatrix}\begin{bmatrix} P \\ V \end{bmatrix} + \begin{bmatrix} 0 \\ S' \end{bmatrix}. \tag{2.7.2}$$

The elimination procedure can be viewed as solving (2.7.2) by a splitting of the solution into two stages. The first stage consists of propagating the solution without absorbtion. In the second stage the system

$$\frac{\partial}{\partial t}\begin{bmatrix} P \\ V \end{bmatrix} = \begin{bmatrix} -\gamma & 0 \\ 0 & -\gamma \end{bmatrix}\begin{bmatrix} P \\ V \end{bmatrix}$$

is solved by a first order differencing scheme

$$\begin{bmatrix} P \\ V \end{bmatrix}^n = \begin{bmatrix} P \\ V \end{bmatrix}^{n^0} - \gamma\,\mathrm{d}t \begin{bmatrix} P \\ V \end{bmatrix}^{n^0} = (1-\gamma\,\mathrm{d}t)\begin{bmatrix} P \\ V \end{bmatrix}^{n^0}$$

The reduction factor is thus equal to $(1-\gamma\,\mathrm{d}t)$.

The reason for the success of the method can be seen by writing (2.7.2) again as a single equation. For constant density without a source term, a substitution of the first line of (2.7.2) into the second gives,

$$\frac{\partial^2 P}{\partial t^2} = c^2\left(\frac{\partial^2 P}{\partial x^2} + \frac{\partial^2 P}{\partial y^2}\right) - 2\gamma\frac{\partial P}{\partial t} - \gamma^2 P \tag{2.7.3}$$

For constant γ this equation has solution of the type

$$\begin{aligned} P(x,t) =& A f_1(n_1 x + n_2 y - ct)\exp[-\gamma x/c] \\ &+ B f_2(n_1' x + n_2' y + ct)\exp[-\gamma x/c] \end{aligned}$$

where $n_1^2 + n_2^2 = n_1'^2 + n_2'^2 = 1$.

This solution has the form of a traveling wave without dispersion but whose amplitude decreases with distance at a frequency independent rate γ/c. A travelling pulse will thus diminish in amplitude without a change of shape. When γ is variable, the effectiveness of the absorbing boundary can be evaluated a priori by using solutions to (2.7.3) by the propagator matrix method (Kosloff and Kosloff, 1986).

2.8. Implementation of a 3D solution scheme

With the current state of computer technology 3D simulations for reflection seismology can be realistically carried out only on the largest supercomputers. The storage requirements may yet be even more demanding because a typical problem would need on the order of gegabytes of active storage. When implementing a 3D algorithm one cannot avoid being well aware of the structure of the computer being used. In the following sections we describe an implementation on a vector computer with multiple CPU's.

2.9. The solution scheme

The 3D solution algorithm includes two parts, namely the calculation of spatial derivatives and the time integration. For example, for the variable

density acoustic wave equation the spatial derivatives are calculated along x, y and z lines respectively according to:

$$R^n = \frac{\partial}{\partial x}\left(\frac{1}{\rho}\frac{\partial P^n}{\partial x}\right) + \frac{\partial}{\partial y}\left(\frac{1}{\rho}\frac{\partial P^n}{\partial y}\right) + \frac{\partial}{\partial z}\left(\frac{1}{\rho}\frac{\partial P^n}{\partial z}\right) \tag{2.9.1}$$

whereas the time integration is performed according to:

$$\dot{P}^{n+1/2} = \dot{P}^{n-1/2} + c^2\rho\,\mathrm{d}t\,(R^n - S^n) \tag{2.9.2}$$

and,

$$P^{n+1} = P^n + \mathrm{d}t\dot{P}^{n+1/2}.$$

The implementation of the solution algorithm utilized both vectorization and parallelism. Vectorization uses pipelining for arithmetic operations. An operation is broken into smaller stages and when a stage is completed for one set of variables, the next set of variables are passed to this stage without waiting for the whole operation to be completed for the first variables. The following is an example of a Fortran loop which is vectorizable:

```
      DO 1 I=1,200
      A(I) = A(I) + B(I) * D(I)
    1 CONTINUE
```

All supercomputers as well as array processors use vectorization.

Parallelism is the ability to do operations in parallel either within a CPU (multiple function units) or between different CPU's. Parallelism in the current algorithm was done through multitasking where a job can be split into tasks which are picked up consecutively by CPU's which are available. An example of loops which are both vectorizable and multitaskable is,

```
      DO 1 J=1,20
      DO 1 I=1,100
      A(I,J) = A(I,J) * A(I,J) + C
    1 CONTINUE
```

The inner loop is vectorizable while the outer loop consists of 20 tasks.

A second factor which needed to be considered is storage management. For a typical 3D problem the size of active storage may be larger than the physical memory of the computer. Therefore an efficient scheme was needed for transferring data back and forth between physical memory and a larger external storage device.

The evaluation of R^n in (2.1.3) requires calculation of derivatives in the X, Y and Z directions respectively. The calculations were carried out by consecutively bringing in groups of data planes of the 3D grid from the external storage device into physical memory, performing the derivative calculations and returning the data back into the external storage device. In designing the solution algorithm we used two types of data accesses, namely along $X-Z$ planes and along $Y-Z$ planes. Calculations on $X-Z$ planes include the following:

(1) $$\frac{\partial}{\partial x}\left(\frac{1}{\rho}\frac{\partial P^n}{\partial x}\right) + \frac{\partial}{\partial z}\left(\frac{1}{\rho}\frac{\partial P^n}{\partial z}\right)$$

(2) time integration $\quad n \rightarrow n+1$

(3) $$\frac{\partial}{\partial x}\left(\frac{1}{\rho}\frac{\partial P^{n+1}}{\partial x}\right).$$

Calculations on $Y-Z$ planes include:

(1) $$\frac{\partial}{\partial y}\left(\frac{1}{\rho}\frac{\partial P^{n+1}}{\partial y}\right) + \frac{\partial}{\partial z}\left(\frac{1}{\rho}\frac{\partial P^{n+1}}{\partial z}\right)$$

(2) time integration $\quad n+1 \rightarrow n+2$

(3) $$\frac{\partial}{\partial y}\left(\frac{1}{\rho}\frac{\partial P^{n+2}}{\partial y}\right)$$

In the calculations vectorization is achieved within data planes whereas parallelism is achieved between planes.

In order to reduce the number of I/O requests when accessing both $X-Z$ and $Y-Z$ planes, we adopted a special pencil shape nodal numbering scheme (fig. 10). A reflection will show that this type of scheme will require fewer requests to transfer a layer of $Y-Z$ planes from/to the external storage device into or from physical memory than with the natural numbering scheme in which points are labeled consecutively in the order of the X, Y and Z directions respectively (e.g. the number of pencils in the Y directions versus the number of points in the Y direction).

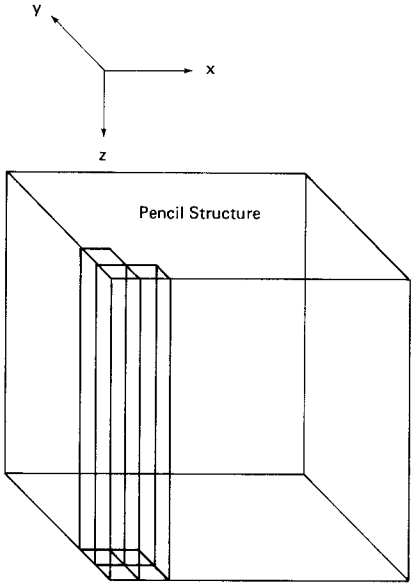

Fig. 10. Pencil data structure for 3D acoustic wave equation.

3. Two and three dimensional elastic forward modeling by the Fourier method

3.1. Momentum conservation and stress–strain relation for an isotropic elastic solid

The elastic forward modeling is based on a direct solution of the equations of momentum conservation combined with the stress–strain relations for a linear isotropic elastic solid undergoing infinitesimal deformation.

Considering two dimensions first, the equations of momentum conservation are given by:

$$\frac{\partial \sigma_{xx}}{\partial x} + \frac{\partial \sigma_{xy}}{\partial y} = \rho \ddot{U}_x + f_x$$

$$\frac{\partial \sigma_{xy}}{\partial x} + \frac{\partial \sigma_{yy}}{\partial y} = \rho \ddot{U}_y + f_y \tag{3.1.1}$$

where U_x and U_y respectively denote the horizontal and vertical displacement components, σ_{xx}, σ_{yy} and σ_{xy} denote the stress components, ρ is the density and f_x and f_y are the body forces. The displacements are related

to the strains by:

$$e_{xx} = \frac{\partial U_x}{\partial x}$$
$$e_{yy} = \frac{\partial U_y}{\partial y}$$
$$e_{xy} = \frac{1}{2}\left(\frac{\partial U_x}{\partial y} + \frac{\partial U_y}{\partial x}\right) \tag{3.1.2}$$

where e_{xx}, e_{yy}, e_{xy} are the strain components. The stress strain relation for an isotropic solid is given by:

$$\sigma_{xx} = (\lambda + 2\mu)e_{xx} + \lambda e_{yy}$$
$$\sigma_{yy} = \lambda e_{xx} + (\lambda + 2\mu)e_{yy},$$
$$\sigma_{xy} = 2\mu e_{xy}. \tag{3.1.3}$$

where σ_{xx}, σ_{yy} and σ_{xy} are the stresses and λ, μ are the rigidity and shear modulus respectively. In 3D the equations of momentum conservation are given by:

$$\rho \ddot{U}_x = \frac{\partial \sigma_{xx}}{\partial x} + \frac{\partial \sigma_{xy}}{\partial y} + \frac{\partial \sigma_{xz}}{\partial z} + f_x$$
$$\rho \ddot{U}_y = \frac{\partial \sigma_{xy}}{\partial x} + \frac{\partial \sigma_{yy}}{\partial y} + \frac{\partial \sigma_{yz}}{\partial z} + f_y$$
$$\rho \ddot{U}_z = \frac{\partial \sigma_{xz}}{\partial x} + \frac{\partial \sigma_{yz}}{\partial y} + \frac{\partial \sigma_{zz}}{\partial z} + f_z \tag{3.1.4}$$

where f_x, f_y, f_z are again the body forces.

The strains are related to the displacements by:

$$e_{xx} = \frac{\partial U_x}{\partial x},$$
$$e_{yy} = \frac{\partial U_y}{\partial y},$$
$$e_{zz} = \frac{\partial U_z}{\partial z}$$
$$e_{xy} = \frac{1}{2}\left(\frac{\partial U_x}{\partial y} + \frac{\partial U_y}{\partial x}\right)$$
$$e_{xz} = \frac{1}{2}\left(\frac{\partial U_x}{\partial z} + \frac{\partial U_z}{\partial x}\right)$$
$$e_{yz} = \frac{1}{2}\left(\frac{\partial U_y}{\partial z} + \frac{\partial U_z}{\partial y}\right). \tag{3.1.5}$$

The stress strain relations are given by:

$$\begin{aligned}
\sigma_{xx} &= \lambda(e_{xx} + e_{yy} + e_{zz}) + 2\mu e_{xx} \\
\sigma_{yy} &= \lambda(e_{xx} + e_{yy} + e_{zz}) + 2\mu e_{yy} \\
\sigma_{zz} &= \lambda(e_{xx} + e_{yy} + e_{zz}) + 2\mu e_{zz} \\
\sigma_{xy} &= 2\mu e_{xy} \\
\sigma_{xz} &= 2\mu e_{xz} \\
\sigma_{yz} &= 2\mu e_{yz} \qquad (3.1.6)
\end{aligned}$$

where λ and μ are again the Lamé constants.

The numerical algorithm solves eqs. (3.1.1)-(3.1.3) (2D) or eqs. (3.1.4)–(3.1.6) (3D). There is also a possibility of solving instead the vector wave equation for the displacements given by:

$$(\lambda + \mu)\nabla(\nabla \boldsymbol{U}) + \mu\nabla(\nabla \boldsymbol{U}) = \rho\nabla^2 \boldsymbol{U} + \boldsymbol{f}.$$

However this equation applies only when the material parameters are constant. Moreover when the terms with derivatives of the material parameters are included in the equation, the overall computational effort will not be less than with the approach adopted in this study. Furthermore, having the rheological relations separate as in (3.1.3) or (3.1.6) allows for substitutions of other more detailed rheologies without affecting the amount of computation considerably.

3.2. Solution algorithm

Denoting $U_x^n = U_x(x, y, t = n\,\mathrm{d}t)$ etc., the calculations in a single time step for 2D include the following:

(1) Calculate:

$$\begin{aligned}
e_{xx}^n &= \frac{\partial U_x^n}{\partial x} \\
e_{yy}^n &= \frac{\partial U_y^n}{\partial y}
\end{aligned}$$

and

$$e_{xy}^n = \frac{1}{2}\left(\frac{\partial U_x^n}{\partial y} + \frac{\partial U_y^n}{\partial x}\right)$$

by the Fourier method.

(2) Calculate:

$$\begin{aligned}
\sigma_{xx}^n &= (\lambda + 2\mu)e_{xx}^n + \lambda e_{yy}^n \\
\sigma_{yy}^n &= \lambda e_{xx}^n + (\lambda + 2\mu)e_{yy}^n \\
\sigma_{xy}^n &= 2\mu e_{xy}^n
\end{aligned}$$

by a multiplication loop.

(3) Calculate:

$$\begin{aligned}
\ddot{U}_x^n &= \frac{1}{\rho}\left(\frac{\partial \sigma_{xx}^n}{\partial x} + \frac{\partial \sigma_{xy}^n}{\partial y} - f_x^n\right) \\
\ddot{U}_y^n &= \frac{1}{\rho}\left(\frac{\partial \sigma_{xy}^n}{\partial x} + \frac{\partial \sigma_{yy}^n}{\partial y} - f_y^n\right),
\end{aligned}$$

using the Fourier method.

(4) Integrate in time:

$$\begin{aligned}
\dot{U}_x^{n+1/2} &= \dot{U}_x^{n-1/2} + \mathrm{d}t \cdot \ddot{U}_x^n \\
\dot{U}_y^{n+1/2} &= \dot{U}_y^{n-1/2} + \mathrm{d}t \cdot \ddot{U}_y^n
\end{aligned}$$

and,

$$\begin{aligned}
U_x^{n+1} &= U_x^n + \mathrm{d}t \cdot \dot{U}_x^{n+1/2} \\
U_y^{n+1} &= U_y^n + \mathrm{d}t \cdot \dot{U}_y^{n+1/2}
\end{aligned}$$

Similar steps are also used for 3D wave propagation.

3.3. Source types

The elastic forward modeling algorithm allows for the introduction of different kinds of seismic sources. We implemented three types namely a directional force, a pressure force and a shear source. All sources used are of the separable type $\boldsymbol{f}(\boldsymbol{x}, t) = \boldsymbol{S}(\boldsymbol{x})h(t)$ where the vector $\boldsymbol{S}(\boldsymbol{x})$ is a localized function of the position vector $\boldsymbol{x}$, and $h(t)$ is the source time history.

Directional force . A directional force vector has components of the type $f_i(\boldsymbol{x}, t) = a(\boldsymbol{x})\delta_{im}h(t)$ where m is the source direction and $a(\boldsymbol{x})$ is a localized function around the source location (can be also $\delta(\boldsymbol{x} - \boldsymbol{x}_0)$ with $\boldsymbol{x}_0$ the source coordinate).

Pressure source . A pressure source is of the form $f_i = \partial\phi/\partial x_i$ where the potential ϕ is of the form $\phi(\boldsymbol{x}) = a(\boldsymbol{x})h(t)$.

$a(\boldsymbol{x})$ is a localized function (usually $\exp[-\alpha((\boldsymbol{x}-\boldsymbol{x}_0)\cdot(\boldsymbol{x}-\boldsymbol{x}_0)]$). This source generates only P waves.

The derivatives must be calculated by the Fourier method and not analytically to assure numerical strain compatibility (Kosloff et al., 1984).

Shear source . A shear source is of the form $\boldsymbol{f} = \operatorname{curl}\boldsymbol{Y}$, with $\boldsymbol{Y}$ a vector potential. In 2D $\boldsymbol{Y} = (0,0,Y)$ with $Y(x,y,t) = a(x,y)h(t)$, where $a(x,y)$ is the same as for the pressure source. This source generates only S waves.

3.4. Stability and numerical dispersion

We examine the two dimensional case for homogeneous material properties and without sources. We first try the P wave solution:

$$\begin{pmatrix} U_x \\ U_y \end{pmatrix} = \begin{pmatrix} k_x \\ k_y \end{pmatrix} \exp[\mathrm{i}(k_x x + k_y y - \omega n\,\mathrm{d}t)] \tag{3.4.1}$$

This solution represents a plane wave traveling in the (k_x, k_y) direction polarized in the direction of propagation. A second order differencing in time yields,

$$\rho\ddot{U}_x^n = \frac{-k_x 4\rho}{\mathrm{d}t^2}\sin^2\frac{\omega\,\mathrm{d}t}{2}\,\mathrm{e}^{\mathrm{i}(k_x x+k_y y-\omega n\,\mathrm{d}t)} = \frac{-4\rho}{\mathrm{d}t^2}\sin^2\frac{\omega\,\mathrm{d}t}{2}U_x^n \tag{3.4.2}$$

$$\rho\ddot{U}_y^n = \frac{-k_y 4\rho}{\mathrm{d}t^2}\sin^2\frac{\omega\,\mathrm{d}t}{2}\,\mathrm{e}^{\mathrm{i}(k_x x+k_y y-\omega n\,\mathrm{d}t)} = \frac{-4\rho}{\mathrm{d}t^2}\sin^2\frac{\omega\,\mathrm{d}t}{2}U_y^n \tag{3.4.3}$$

The strains corresponding to eq. (3.4.1) are given by,

$$e_{xx}^n = \frac{\partial U_x^n}{\partial x} = +\mathrm{i}k_x^2\,\mathrm{e}^{\mathrm{i}(k_x x+k_y y-\omega n\,\mathrm{d}t)}$$

$$e_{yy}^n = \frac{\partial U_y^n}{\partial y} = +\mathrm{i}k_y^2\,\mathrm{e}^{\mathrm{i}(k_x x+k_y y-\omega n\,\mathrm{d}t)}$$

and,

$$e_{xy}^n = \frac{1}{2}\left(\frac{\partial U_x^n}{\partial y} + \frac{\partial U_y^n}{\partial x}\right) = +\mathrm{i}k_x k_y\,\mathrm{e}^{\mathrm{i}(k_x x+k_y y-\omega n\,\mathrm{d}t)}$$

Hence the stresses become,

$$\sigma_{xx}^n = (\lambda+2\mu)e_{xx} + \lambda e_{yy}^n = \left[\mathrm{i}(\lambda+2\mu)k_x^2 + \mathrm{i}\lambda k_y^2\right]e^{\mathrm{i}(k_x x+k_y y-\omega n\,\mathrm{d}t)}$$

$$\sigma_{yy}^n = \lambda e_{xx}^n + (\lambda+2\mu)e_{yy}^n = \left[\mathrm{i}\lambda k_x^2 + \mathrm{i}(\lambda+2\mu)k_y^2\right]e^{\mathrm{i}(k_x x+k_y y-\omega n\,\mathrm{d}t)}$$

and,

$$\sigma_{xy}^n = 2\mu e_{xy}^n = \mathrm{i}2\mu k_x k_y e^{\mathrm{i}(k_x x+k_y y-\omega n\,\mathrm{d}t)}. \tag{3.4.4}$$

Based on these values, the evaluation of the left hand side of the equations of conservation of momentum gives,

$$\begin{aligned}\frac{\partial\sigma_{xx}^n}{\partial x} + \frac{\partial\sigma_{yy}^n}{\partial y} &= -\left[(\lambda+2\mu)k_x^3 + \lambda k_x k_y^2\right]\mathrm{e}^{\mathrm{i}(k_x x+k_y y-\omega n\,\mathrm{d}t)} \\ &\quad - 2\mu k_x k_y^2\,\mathrm{e}^{\mathrm{i}(k_x x+k_y y-\omega n\,\mathrm{d}t)} \\ &= -(\lambda+2\mu)(k_x^2+k_y^2)U_x^n \end{aligned}\tag{3.4.5}$$

Similarly:

$$\frac{\partial\sigma_{xy}}{\partial x} + \frac{\partial\sigma_{yy}}{\partial y} = -(\lambda+2\mu)(k_x^2+k_y^2)U_y^n$$

In order to satisfy the equations of momentum conservation (3.1.1), we must have,

$$(\lambda+2\mu)(k_x^2+k_y^2) = \frac{4\rho}{\mathrm{d}t^2}\sin^2\frac{\omega\,\mathrm{d}t}{2} \tag{3.4.6}$$

or

$$(k_x^2+k_y^2)^{1/2} = \frac{2}{V_p\,\mathrm{d}t}\sin\frac{\omega\,\mathrm{d}t}{2}$$

Where $V_p = \sqrt{(\lambda+2\mu)/\rho}$ is the P wave velocity. This is the same dispersion relation as in the acoustic case. Therefore all the conclusions regarding stability and numerical dispersion will remain the same as in that case. A similar calculation for an S wave solution,

$$\begin{pmatrix} U_x \\ U_y \end{pmatrix} = \begin{pmatrix} -k_y \\ k_x \end{pmatrix}\mathrm{e}^{(k_x x+k_y y-\omega n\,\mathrm{d}t)} \tag{3.4.7}$$

yields the relation

$$(k_x^2+k_y^2)^{1/2} = \frac{2}{V_s\,\mathrm{d}t}\sin\frac{\omega\,\mathrm{d}t}{2}$$

where $V_s = \sqrt{\mu/\rho}$. Because the S wave velocity is always smaller than the P wave velocity, the considerations regarding stability and dispersion should be based on the P wave velocity. However, the highcut frequency which is derived on the basis of the lowest velocity should be according to the S velocities. The same type of analysis as above can be carried out for the 3D case.

3.5. Free surface boundary condition

As with the acoustic case the free surface boundary condition is approximated by a wide zone bellow the grid with zero P and S velocities. Although this means that all stress components are zero in that region, the velocities as well as the displacements are not zero there and must be stored (usually they are almost equal to zero as we move away from the boundaries). Doubts have been raised about the correctness of this condition since the correct boundary condition requires the vanishing of the tractions only, and not of all the stress components as in the present procedure. For example in 2D $t_x = \sigma_{xy}$ and $t_y = \sigma_{yy}$ should vanish but not necessarily σ_{xx}. Indeed tests which we have performed indicate that this condition is not perfect when the source and receivers are close to the surface, but seems to work well when the source and receivers are well bellow the surface.

3.6. Conservation of energy

Most theorems of linear elasticity can be proven independently for the Fourier method with the second order time derivative approximation. At first we derive the law of energy conservation. The derivations are carried out in the following for 2D geometry. A similar analysis can also be done for 3D.

For the sake of brevity we use subscript notation with the convention where a repeated index implies summation. The equation of momentum conservation then writes:

$$\frac{\partial \sigma_{ij}}{\partial x_j} = \rho \ddot{U}_i + f_i \qquad i = 1, 2$$

The displacement strain relation is given by:

$$e_{ij} = \frac{1}{2}\left(\frac{\partial U_i}{\partial x_j} + \frac{\partial U_j}{\partial x_i}\right) \qquad i, j = 1, 2$$

The stress strain relation reads:

$$\sigma_{ij} = \lambda e_{kk}\delta_{ij} + 2\mu e_{ij}$$

or also

$$\sigma_{ij} = (\lambda \delta_{ij}\delta_{kl} + \mu(\delta_{il}\delta_{jk} + \delta_{ik}\delta_{jl}))e_{kl}.$$

With this form the following lemma is clear,

Lemma 1. *For two different displacement states $U_i^{(1)}, U_i^{(2)}$ with corresponding strains and stresses $e_{ij}^{(1)}\sigma_{ij}^{(1)}$ and $e_{ij}^{(2)}\sigma_{ij}^{(2)}$ respectively, the following relation is satisfied:*

$$\sigma_{ij}^{(1)} e_{ij}^{(2)} = \sigma_{ij}^{(2)} e_{ij}^{(1)}.$$

We will also need the following lemmas:

Lemma 2. *For odd based FFT's and the Fourier derivative approximation,*

$$\sum_{n=0}^{N_x - 1} \frac{\mathrm{d}f}{\mathrm{d}x} = 0$$

Proof: For the DFT, in general,

$$\sum_{n=0}^{N_x - 1} G(x) = \tilde{G}(0)$$

but:

$$\left(\widetilde{\frac{\mathrm{d}f}{\mathrm{d}x}}\right)_{k=0} = \mathrm{i}k\tilde{f}(k)|_{k=0} = 0$$

Lemma 3. *For the DFT derivative approximation, the product rule holds*

$$\frac{\mathrm{d}}{\mathrm{d}x}(f \cdot g) = \frac{\mathrm{d}f}{\mathrm{d}x} \cdot g + f \cdot \frac{\mathrm{d}g}{\mathrm{d}x}$$

Proof: By the convolutional property:

$$\frac{\mathrm{d}}{\mathrm{d}x}(f \cdot g) \Rightarrow \mathrm{i}k\widetilde{(fg)} = \mathrm{i}kN_x \tilde{f} * \tilde{g}$$

where the $*$ symbol denotes a convolution. Therefore,

$$\begin{aligned}\frac{\mathrm{d}}{\mathrm{d}x}(f\cdot g) \Rightarrow & N_x \sum_{\nu'=-(N_x-1)/2}^{(N_x-1)/2} \mathrm{i}k_\nu \tilde{f}(k_{\nu'})\tilde{g}(k_\nu - k_{\nu'}) \\ &= N_x \sum_{\nu=-(N_x-1)/2}^{(N_x-1)/2} \mathrm{i}k'_\nu \tilde{f}(k_{\nu'})\tilde{g}(k_\nu - k_{\nu'}) \\ &+ N_x \sum_{\nu'=-(N_x-1)/2}^{(N_x-1)/2} \mathrm{i}\tilde{f}(k_{\nu'})(k_\nu - k'_\nu)\tilde{g}(k_\nu - k_{\nu'}) \\ &= \left(\widetilde{\frac{\mathrm{d}f}{\mathrm{d}x}}\cdot g\right) + \left(f\cdot \widetilde{\frac{\mathrm{d}g}{\mathrm{d}x}}\right)\end{aligned}$$

As a result of lemma 2 and lemma 3 we get the discrete equivalent of Gauss's theorem;

Lemma 4. *For two discrete and periodic functions f and g*

$$\sum_{n=0}^{N_x-1} f_n \cdot \frac{\mathrm{d}g_n}{\mathrm{d}x} = -\sum_{n=0}^{N_x-1} \frac{\mathrm{d}f_n}{\mathrm{d}x}\cdot g_n$$

and in two dimensions

$$\sum_{n_y=0}^{N_y-1}\sum_{n_x=0}^{N_x-1} f_{n_x n_y}\frac{\partial g_{n_x n_y}}{\partial x} = -\sum_{n_y=0}^{N_y-1}\sum_{n_x=0}^{N_x-1}\frac{\partial f_{n_x n_y}}{\partial x} g_{n_x n_y}$$

or in general

$$\sum_{n_y=0}^{N_y-1}\sum_{n_x=0}^{N_x-1} f_{n_x n_y}\frac{\partial g_{n_x n_y}}{\partial x_i} = -\sum_{n_y=0}^{N_y-1}\sum_{n_x=0}^{N_x-1}\frac{\partial f_{n_x n_y}}{\partial x_i} g_{n_x n_y}.$$

We now need a number of results concerning temporal derivatives. We denote:

$$\begin{aligned}\dot{U}_i^n &= \frac{1}{2}\left(\dot{U}_i^{n+1/2} + \dot{U}_i^{n-1/2}\right) \\ &= \frac{1}{2}\frac{U_i^{n+1}-U_i^n}{\mathrm{d}t} + \frac{1}{2}\frac{U_i^n - U_i^{n-1}}{\mathrm{d}t} \\ &= \frac{U_i^{n+1}-U_i^{n-1}}{2\,\mathrm{d}t}\end{aligned}$$

where,

$$\dot{U}_i^{n+1/2} = \frac{U_i^{n+1}-U_i^n}{\mathrm{d}t}.$$

Since,

$$\ddot{U}_i^n = \frac{1}{\mathrm{d}t}\left(\dot{U}_i^{n+1/2} - \dot{U}_i^{n-1/2}\right)$$

we get

$$\dot{U}_i^n \cdot \ddot{U}_i^n = \frac{1}{2\,\mathrm{d}t}\left[\left(\dot{U}_i^{n+1/2}\right)^2 - \left(\dot{U}_i^{n-1/2}\right)^2\right]. \tag{3.6.1}$$

We can now state the theorems of energy conservation.

Theorem A. *In the absence of body forces the following relation holds:*

$$\sum_{N_x}\sum_{N_y} e_{ij}^{n+1}\sigma_{ij}^n + \sum_{N_x}\sum_{N_y}\rho\dot{U}_i^{n+\frac{1}{2}}\dot{U}_i^{n+\frac{1}{2}} = \text{Const.}$$

This is the analogue of continuum relation:

$$\frac{\mathrm{d}}{\mathrm{d}t}\left[\int_V \sigma_{ij}e_{ij}\,\mathrm{d}v + \int_V \rho\dot{U}_i\dot{U}_i\,\mathrm{d}V\right] = 0,$$

in the absence of body force or external tractions. The first term represents potential energy whereas the second term gives the kinetic energy.

Proof: Multiply the equation of momentum conservation in the absence of body forces by $\dot{U}_i^n$ and sum over $N_x N_y$

$$\sum_{N_x}\sum_{N_y}\dot{U}_i^n\frac{\partial\sigma_{ij}^n}{\partial x_j} = \sum_{N_x}\sum_{N_y}\rho\dot{U}_i^n\ddot{U}_i^n$$

using lemma 4 and (3.6.1) we can write:

$$-\sum_{N_x}\sum_{N_y}\frac{\partial\dot{U}_i^n}{\partial x_j}\sigma_{ij}^n = \sum_{N_x}\sum_{N_y}\rho\frac{\dot{U}_i^{n+1/2}\dot{U}_i^{n+1/2} - \dot{U}_i^{n-1/2}\dot{U}_i^{n-1/2}}{2\,\mathrm{d}t}$$

Using the symmetry of σ_{ij}^n, and then Lemma 1 we can write:

$$\frac{\partial \dot{U}_i^n}{\partial x_j}\sigma_{ij}^n = \dot{e}_{ij}^n \sigma_{ij}^n = \frac{e_{ij}^{n+1} - e_{ij}^{n-1}}{2\,\mathrm{d}t}\sigma_{ij}^n = \frac{\sigma_{ij}^{n+1}e_{ij}^n - \sigma_{ij}^n e_{ij}^{n-1}}{2\,\mathrm{d}t}$$

therefore:

$$-\sum_{N_x}\sum_{N_y}\frac{\sigma_{ij}^{n+1}e_{ij}^n - \sigma_{ij}^n e_{ij}^{n-1}}{2\,\mathrm{d}t} = \sum_{N_x}\sum_{N_y}\rho\frac{\dot{U}_i^{n+1/2}\dot{U}_i^{n+1/2} - \dot{U}_i^{n-1/2}\dot{U}_i^{n-1/2}}{2\,\mathrm{d}t}$$

or

$$\sum_{N_x}\sum_{N_y}\sigma_{ij}^{n+1}e_{ij}^n + \sum_{N_x}\sum_{N_y}\rho\dot{U}_i^{n+1/2}\dot{U}_i^{n+1/2} = \sum_{N_x}\sum_{N_y}\sigma_{ij}^n e_{ij}^{n-1} + \sum_{N_x}\sum_{N_y}\rho\dot{U}_i^{n-1/2}\dot{U}_i^{n-1/2},$$

which states that this quantity is constant as it does not change between time steps.

Theorem B. *When body forces are present and for zero initial conditions*

$$\sum_{N_x}\sum_{N_y}\sigma_{ij}^{n+1}e_{ij}^n + \sum_{N_x}\sum_{N_y}\rho\dot{U}_i^{n+1/2}\dot{U}_i^{n+1/2} = -\sum_{\alpha=0}^{n}\sum_{N_x}\sum_{N_y}\dot{U}_i^\alpha f_i^\alpha$$

The right hand side represents the total work of the body forces.

Proof: Again, multiply the momentum conservation equation by $\dot{U}_i^n$, but this time with the body force term included. We get:

$$\frac{1}{2}\sum_{N_x}\sum_{N_y}\dot{U}_i^n\frac{\partial\sigma_{ij}^n}{\partial x_j} = \frac{1}{2}\sum_{N_x}\sum_{N_y}\rho\dot{U}_i^n\dot{U}_i^n - \sum_{N_x}\sum_{N_y}\dot{U}_i^n f_i^n\,\mathrm{d}t$$

and with the same manipulations as for theorem A we get:

$$-\sum_{N_x}\sum_{N_y}\frac{\sigma_{ij}^{n+1}e_{ij}^n - \sigma_{ij}^n e_{ij}^{n-1}}{2\,\mathrm{d}t} = \sum_{N_x N_y}\frac{\rho}{2\,\mathrm{d}t}\left[\dot{U}_i^{n+1/2}\dot{U}_i^{n+1/2} - \dot{U}_i^{n-1/2}\dot{U}_i^{n-1/2}\right] + \sum_{N_x}\sum_{N_y}\dot{U}_i^n f_i^n$$

Replacing n by α and summing over time from 0 to n gives:

$$-\sum_{\alpha}^{n}\sum_{N_x}\sum_{N_y}\mathrm{d}t\dot{U}_i^\alpha f_i^\alpha = \frac{1}{2}\sum_{N_x}\sum_{N_y}\left[\sigma_{ij}^{n+1}e_{ij}^n + \rho\dot{U}_i^{n+1/2}\dot{U}_i^{n+1/2}\right]$$

which is the required result. The energy conservation has been checked numerically and found to be valid to within computer precision.

3.7. Source receiver reciprocity

The Fourier method satisfies source receiver reciprocity as in the continuous case. Given one solution U_i^m corresponding to a point force in the m direction at location (i_1, j_1), and a second displacement V_j^l corresponding to a point source in the l direction located at (i_2, j_2) with the same wavelet then:

$$U_l^m(i_2, j_2) = V_m^l(i_1, j_1)$$

(Here the superscript denotes force direction and does not correspond to the time variable as previously).

Proof: We prove the results first for an impulsive force and then, because of the superposition, the result will be true for any wavelet. The displacements from the first set of forces satisfy:

$$\frac{\partial\sigma_{ij}^m}{\partial x_j} = \rho\ddot{U}_i^m + \delta_{im}\delta(I - i_1)\delta(J - j_1)\delta(n) \tag{3.7.1}$$

where as before

$$U_i^m(I, J, n) = U_i(X = I\,\mathrm{d}x, y = J\,\mathrm{d}y, t = n\,\mathrm{d}t)$$

The second set of displacements satisfy:

$$\frac{\partial\tau_{ij}^l}{\partial x_j} = \rho\ddot{V}_i^l + \delta_{il}\delta(I - i_2)\delta(J - j_2)\delta(O) \tag{3.7.2}$$

where we have used a different time index O. We now multiply (3.7.1) by V_i^l and (3.7.2) by U_i^m, subtract the results, and perform a summation over all grid points to get:

$$\sum_I\sum_J\left[V_i^l\frac{\partial\sigma_{ij}^m}{\partial x_j} - U_i^m\frac{\partial\tau_{ij}^l}{\partial x_j}\right] = \sum_I\sum_J\left[\rho V_i^l\ddot{U}_i^m - \rho U_i^m\ddot{V}_i^l\right] + \sum_I\sum_J\left[V_i^l\delta_{im}\delta(I - i_1)\delta(J - j_1)\delta(n) - U_i^l\delta_{il}\times\delta(I - i_2)\delta(J - j_2)\delta(O)\right]$$

or using the discrete Gauss's theorem,

$$-\sum_I\sum_J\left[\frac{\partial V_i^l}{\partial x_j}\sigma_{ij}^m-\frac{\partial U_i^m}{\partial x_j}\tau_{ij}^l\right]$$
$$=\sum_I\sum_J\left[\rho V_i^l\ddot{U}_i^m-\rho U_i^m\ddot{V}_i^l\right]+V_m^l(i_1,j_1,0)\delta(n)-U_l^m(i_2,j_2,n)\delta(O)$$

However,

$$\sum_I\sum_J\left[\frac{\partial V_i^l}{\partial x_j}\sigma_{ij}^m-\frac{\partial U_i^m}{\partial x_j}\tau_{ij}^l\right]=\sum_I\sum_J\left[\epsilon_{ij}^l\sigma_{ij}^m-e_{ij}^m\tau_{ij}^l\right]$$

where we utilized the symmetry of σ_{ij}, τ_{ij} and replaced $\partial U_i^m/\partial x_j$, $\partial V_i^l/\partial x_j$ by the corresponding strains e_{ij}^m and ϵ_{ij}^l respectively. The term vanishes because:

$$\epsilon_{ij}^l\sigma_{ij}^m=\tau_{ij}^l e_{ij}^m$$

We next replace the time index 0 by $\tau-n$ and sum from zero to τ. We get:

$$\sum_I\sum_J\left[\sum_{n=0}^{\tau}\rho V_i^l(I,J,\tau-n)\ddot{U}_i^m(I,J,n)-\rho U_i^m(I,J,n)\ddot{V}_i^l(I,J,\tau-n)\right]$$
$$+\sum_{n=0}^{\tau}\left[V_i^l(i_1,j_1,\tau-n)\delta(n)-U_i^m(i_2,j_2,n)\delta(\tau-n)\right]=0$$

We now evaluate:

$$\sum_{n=0}^{\tau}\left[\rho V_i^l(I,J,\tau-n)\ddot{U}_i^m(I,J,n)-\rho U_i^m(I,J,n)\ddot{V}_i^l(I,J,\tau-n)\right]$$
$$=\sum_{n=0}^{\tau}\Bigg[\rho V_i^l(I,J,\tau-n)$$
$$\times\frac{U_i^m(I,J,n+1)-2U_i^m(I,J,n)+U_i^m(I,J,n-1)}{\mathrm{d}t^2}$$
$$-\rho U_i^m(I,J,n)$$
$$\times\frac{V_i^l(I,J,\tau-n-1)-2V_i^l(I,J,\tau-n)+V_i^l(I,J,\tau-n+1)}{\mathrm{d}t^2}\Bigg]$$
$$=\frac{1}{\mathrm{d}t^2}\sum_{n=0}^{\tau}\Big[\rho V_i^l(I,J,\tau-n)U_i^m(I,J,n+1)$$
$$-\rho V_i^l(I,J,\tau-n-1)U_i^m(I,J,n)-\rho U_i^m(I,J,n)V_i^l(I,J,\tau-n+1)$$
$$+\rho U_i^m(I,J,n-1)V_i^l(I,J,\tau-n)\Big] \qquad (3.7.3)$$

This sum contains differences of identical terms which are only shifted apart by one index. This sum must therefore vanish if $U_i^m(I,J,0)=V_i^l(I,J,0)=U_i^m(I,J,1)=V_i^l(I,J,1)=0$, which corresponds to zero initial conditions for displacements and velocities (since $\dot{U}_i^m(I,J,0)=\left[U_i^l(I,J,1)-U^l(I,J,-1)\right]/2\,\mathrm{d}t$ etc). Performing the remaining sum in (3.7.3) then gives:

$$V_m^l(i_1,j_1,\tau)=U_l^m(i_2,j_2,\tau)$$

which proves the theorem.

Reciprocity has been verified on the computer to within the accuracy of the machine.

4. Improvement of the time integration

Until now we have compared spatial derivative approximations while always using second order differencing for the time derivative approximation. However, due to a recent development by Tal-Ezer (1984), the time integration can be carried out with very good accuracy and with better efficiency than by differencing. The basic idea behind Tal-Ezer's approach is that results from approximation theory concerning scalar functions apply directly to linear operators, like the operators encountered in the spatial derivative approximation for the wave equations. In the following we illustrate the theory for the 1D constant density wave equation. The results apply directly to 2D and 3D as well as to the elastic wave propagation.

4.1. The formal solution

We consider the 1D acoustic wave equation given by:

$$\frac{1}{c^2}\frac{\partial^2 P}{\partial t^2}=\frac{\partial^2 P}{\partial x^2}+S \qquad (4.1.1)$$

and write it as a coupled system:

$$\frac{\partial}{\partial t}\begin{bmatrix}P\\ \frac{\partial P}{\partial t}\end{bmatrix}=\begin{bmatrix}0 & 1\\ c^2\frac{\partial^2}{\partial x^2} & 0\end{bmatrix}\begin{bmatrix}P\\ \frac{\partial P}{\partial t}\end{bmatrix}+\begin{bmatrix}0\\ c^2S\end{bmatrix} \qquad (4.1.2)$$

With a suitable approximation for the spatial derivatives this system becomes a set of $2N_x$ coupled ordinary differential equations in time for P

and $\partial P/\partial t$ at the N_x spatial grid points. This system can be written in compact form:

$$\frac{\mathrm{d}\boldsymbol{V}}{\mathrm{d}t} = G_n \boldsymbol{V} + \boldsymbol{f} \tag{4.1.3}$$

subject to the initial condition $\boldsymbol{V}(t=0) = \boldsymbol{V}^0$. $\boldsymbol{V}$ is a vector of size $2N_x$ of P and $\dot{P}$ at the grid points, $\boldsymbol{f}$ is the inhomogeneous term in (4.1.2) and G_n is the discrete representation of the operator in that equation. The formal solution to (4.1.3) is given by:

$$\boldsymbol{V}(t) = \mathrm{e}^{tG_n}\,\boldsymbol{V}^0 + \int_0^t \mathrm{e}^{tG_n}\,\boldsymbol{f}(t-\tau)\,\mathrm{d}\tau. \tag{4.1.4}$$

This solution has the same form as the solution when $\boldsymbol{V}$, $\boldsymbol{f}$ and G_n are scalars. In the following we consider a Chebychev expansion of (4.1.4) which is both accurate and also gives continuous error control. The homogeneous case with no source term is first discussed.

4.2. Homogeneous case

We use the following known expansion for e^z:

$$\mathrm{e}^z \approx \sum_{k=0}^{M} C_k J_k(tR) Q_k\left(\frac{z}{tR}\right), \tag{4.2.1}$$

where $|z| < tR$ and z lies close to the imaginary axis. $C_0 = 1$ and $C_k = 2$ for $k \neq 0$. J_k represents the Bessel function of order k and $Q_k(\omega)$ are modified Chebychev polynomials which satisfy the recurrence relation:

$$Q_{k+1}(\omega) = 2\omega Q_k(\omega) + Q_{k-1}(\omega) \tag{4.2.2}$$

with $Q_0 = 1$ and $Q_1 = \omega$ (Tal-Ezer,1984). Generally the series converges rapidly for $M > tR$. Using tG_n instead of z results in the approximate solution:

$$\boldsymbol{V}(t) = \sum_{k=0}^{M} C_k J_k(tR) Q_k\left(\frac{G_n}{R}\right)\boldsymbol{V}^0. \tag{4.2.3}$$

R should be chosen larger than the range of the eigenvalues of G_n. Based on the homogeneous velocity case where the eigenvalues can be shown to

be $\pm \mathrm{i}ck_\nu$ with k_ν the wavenumber (the corresponding eigenvectors are, $(1, \mathrm{e}^{\mathrm{i}k_\nu}, \mathrm{e}^{2\mathrm{i}k_\nu}, \ldots, \mathrm{e}^{\mathrm{i}k_\nu(N_x-1)}, \pm\mathrm{i}ck_\nu, \pm\mathrm{i}ck_\nu\ \mathrm{e}^{\mathrm{i}k_\nu} \ldots . \pm\mathrm{i}ck_\nu\ \mathrm{e}^{\mathrm{i}k_\nu(N_x-1)})$, $\nu = -N_x/2, \ldots, (N_x-1)/2$ for even based DFT). R should be chosen slightly larger than $c_{\max}\pi/\,\mathrm{d}x$. The solution in (4.2.3) can be generated recursively. The starting values are given by:

$$Q_0\left(\frac{G_n}{R}\right)\boldsymbol{V}^0 = \boldsymbol{V}^0 \tag{4.2.4}$$

and

$$Q_1\left(\frac{G_n}{R}\right)\boldsymbol{V}^0 = \frac{G_n}{R}\boldsymbol{V}^0$$

Additional terms are generated with G_n/R replacing ω in (4.2.2). Each time after a new Q_k is calculated, an additional term is added to the sum (4.2.3). After $\boldsymbol{V}(t)$ has been calculated, it can be used as a starting value to step the solution once more. The algorithm becomes more efficient for large time increments although then the storage required for snapshots and time sections may increase considerably.

4.3. Intermediate results

Equation (4.2.3) shows how to step the solution from 0 to time t in a relatively large increment (often $Rt \approx 100$ or $t \approx 200$ msec). However, especially for time sections we need results at much smaller intervals. To achieve this we use (4.2.3) with $t' < t$ replacing t. This does require calculation of other sets of Bessel functions $J_k(t'R)$, (a relatively inexpensive scalar operation) but does not require the calculation of new Chebychev vector polynomials $Q_k\boldsymbol{V}^0$, which is the most costly operation.

4.4. Solution with source term

As in the previous sections, we consider a separable source of the form

$$\boldsymbol{f}(t) = \boldsymbol{A}h(t) \tag{4.4.1}$$

where $\boldsymbol{A}(\boldsymbol{x})$ is a time independent vector. $\boldsymbol{A}(\boldsymbol{x})$ is usually chosen to be a δ-function or at least a highly localized function in space. $h(t)$ gives the source time history. The inhomogeneous solution then becomes:

$$\boldsymbol{V} = \left[\int_0^t \mathrm{e}^{\tau G_n}\,h(t-\tau)\,\mathrm{d}\tau\right]\boldsymbol{A}. \tag{4.4.2}$$

Using the Chebychev expansion for the exponential we get:

$$\boldsymbol{V} = \sum_{k=0}^{M} \left[\int_0^t C_k J_k(\tau R) h(t-\tau)\,\mathrm{d}\tau \right] Q_k \left[\frac{G_n}{R} \right] \boldsymbol{A}. \tag{4.4.3}$$

This has the same form as the homogeneous case except that $\boldsymbol{A}$ replaces $\boldsymbol{V}^0$ and the Bessel functions $J_k(tR)$ are replaced by the coefficients:

$$b_k = \int_0^t J_k(\tau R) h(t-\tau)\,\mathrm{d}\tau \tag{4.4.4}$$

The coefficients b_k need to be calculated by numerical integration.

4.5. Nonreflecting boundary condition

We have seen that the absorbing boundary could be represented by replacing the acoustic wave equation by the system:

$$\frac{\mathrm{d}}{\mathrm{d}t} \begin{bmatrix} P \\ V \end{bmatrix} = \begin{bmatrix} -\gamma & 1 \\ c^2 \frac{\partial^2}{\partial x^2} & -\gamma \end{bmatrix} \begin{bmatrix} P \\ V \end{bmatrix} + \begin{bmatrix} 0 \\ c^2 S \end{bmatrix}.$$

When incorporating the nonreflecting boundary condition with the Tal-Ezer method this system is solved directly. γ is different from zero only along the boundaries of the grid. γ causes the eigenvalues of G_n to have a real negative component (when γ is uniform they are simply shifted by γ). This in turn, may necessitate the expansion R considerably to ensure convergence of the expansion. Instead it is possible to modify the scheme somewhat according to:

$$\boldsymbol{V} = \mathrm{e}^{G_n t}\, \boldsymbol{V}^0 = \mathrm{e}^{-\lambda t I}\, \mathrm{e}^{t(G_n + \lambda I)}\, \boldsymbol{V}^0$$

where λ is a suitably chosen shift parameter and I is the $2N_x \times 2N_x$ identity matrix. Then $\mathrm{e}^{t(G_n+\lambda I)}$ is expanded and the results are multiplied by $\mathrm{e}^{-\lambda I t}$ after the calculation. We have found that the value $\lambda = \gamma_{\max}/2$ works well.

4.6. Efficiency, comparisons with finite differences

It is interesting to compare the efficiency of the Tal-Ezer method with the efficiency of temporal differencing. The key factor in comparing computational effort is the required number of spatial derivative evaluations required in propagating the solution a certain amount of time. For temporal differencing this amounts to the required number of time steps whereas

for the Tal-Ezer method this amounts to the number of terms in the Chebychev expansion. For the comparison we consider the amount of effort for propagating the solution 100 grid lengths in a homogeneous model.

Temporal differencing with $\alpha = c\,\mathrm{d}t/\mathrm{d}x = 0.2$ obviously requires 500 function evaluations. On the other hand for the Tal-Ezer method the number of functional evaluations N_f is approximately tR. Here $t = 100\,\mathrm{d}x/c$ whereas for 1D $R = c\pi/\mathrm{d}x$. Therefore, $N_f = 100\pi \approx 314$ function evaluations. For 2D, this value needs to multiplied by $\sqrt{2}$ to yield approximately 441. In 3D the 1D value needs to be multiplied by $\sqrt{3}$ thus giving 544.

As for storage, the Tal-Ezer method requires storing $\boldsymbol{V}, Q_k\boldsymbol{V}$, and $Q_{k-1}\boldsymbol{V}$ which are of size $2N_x$ and c which requires N_x words. This amounts to 7 variables of size N_x which is significantly more than the 4 variables required for differencing. In a later section we will derive variants of the Tal-Ezer method which are both faster and require less storage.

5. Forward modeling from an operator view

The time integration method introduced by Tal-Ezer (1984) was based on the analogy between solutions to the first order scalar ordinary differential equation $\mathrm{d}Y/\mathrm{d}t = gY$ and the coupled equations which are obtained after a spatial discretization of the wave equation. This suggests a reexamination of numerical modeling from an operator perspective. The following sections are a first attempt in this direction.

5.1. The formal solution

We return to the acoustic wave equation for constant density:

$$\frac{\partial^2 P}{\partial t^2} = c^2(x)\frac{\partial^2 P}{\partial x^2} + S(x)h(t) \tag{5.1.1}$$

where $S(x)$ is the source spatial distribution, and $h(x)$ is the source time history. We rewrite this equation as:

$$\frac{\partial^2 \boldsymbol{P}}{\partial t^2} = -L_{N_x}^2 \boldsymbol{P} + \boldsymbol{S}(x)h(t) \tag{5.1.2}$$

where

$$-L_{N_x}^2 = c^2 \frac{\partial^2}{\partial x^2}$$

is a spatial operator. After spatial discretization, (5.1.2) becomes a coupled system of N_x ordinary differential equations for the vector $\boldsymbol{P}$ containing the nodal pressures. The formal solution of (5.1.2) without the source term is

$$\boldsymbol{P}_t = \cos[L_{N_x} t]\boldsymbol{P}_0 + \frac{\sin[L_{N_x} t]}{L_{N_x}} \dot{\boldsymbol{P}}_0 \tag{5.1.3}$$

Equation (5.1.3) satisfies (5.1.2) and also

$$\boldsymbol{P}(t=0) = \boldsymbol{P}_0,$$

and

$$\frac{\partial \boldsymbol{P}}{\partial t}(t=0) = \dot{\boldsymbol{P}}_0 .$$

This type of approach was already used in a previous section discussing the Tal-Ezer method. However there the point of departure was the coupled system:

$$\frac{\partial}{\partial t}\begin{bmatrix} P \\ \frac{\partial P}{\partial t} \end{bmatrix} = \begin{bmatrix} 0 & 1 \\ c^2 \frac{\partial^2}{\partial x^2} & 0 \end{bmatrix} \begin{bmatrix} P \\ \frac{\partial P}{\partial t} \end{bmatrix} + \begin{bmatrix} 0 \\ S(x)h(t) \end{bmatrix}, \tag{5.1.4}$$

or in operator notation,

$$\frac{\partial \boldsymbol{V}}{\partial t} = G_{N_x} \boldsymbol{V} + \boldsymbol{f} h(t)$$

where

$$\boldsymbol{f}^T = (0, 0, \ldots, 0, S(0), S(1), \ldots, S(N_x - 1))$$

and

$$\boldsymbol{V}_{N_x}^T = \left(P(0,t), P(1,t), \ldots, P(N_x - 1, t), \frac{\partial P}{\partial t}(0,t), \ldots, \frac{\partial P}{\partial t}(N_x - 1, t) \right)$$

The formal solution to the system without source was shown to be:

$$\boldsymbol{V}_t = \mathrm{e}^{G_n t} \boldsymbol{V}_0 \tag{5.1.5}$$

which satisfies (5.1.4) subject to the initial condition $\boldsymbol{V}_{t=0} = \boldsymbol{V}_0$.

5.2. Rederivation of temporal differencing through a Taylor expansion of the formal solution

Temporal differencing schemes can be obtained after a Taylor expansion of the formal solutions (5.1.3) or (5.1.5). For the single system we can use the series:

$$\begin{aligned} \cos[L_{N_x} t] &= I - \frac{L_{N_x}^2 t^2}{2} + \frac{L_{N_x}^4 t^4}{4!} + \cdots \\ \sin[L_{N_x} t] &= L_{N_x} - \frac{L_{N_x}^3 t^3}{3!} + \frac{L_{N_x}^5 t^5}{5!} + \cdots \end{aligned} \tag{5.2.1}$$

where I is the identity operator. Equation (5.1.3) becomes:

$$\boldsymbol{P}_t = \left[I - \frac{L_{N_x}^2 t^2}{2} + \frac{L_{N_x}^4 t^4}{4!} + \cdots \right] \boldsymbol{P}_0 + \left[t - \frac{L_{N_x}^2 t^3}{3!} + \frac{L_{N_x}^4 t^5}{5!} + \cdots \right] \dot{\boldsymbol{P}}_0$$

For obtaining a formula that does not contain $\dot{P}_0$ we rewrite the above solution for time $-t$:

$$\boldsymbol{P}_{-t} = \left[I - \frac{L_{N_x}^2 t^2}{2} + \frac{L_{N_x}^4 t^4}{4!} + \cdots \right] \boldsymbol{P}_0 - \left[t - \frac{L_{N_x}^2 t^3}{3!} + \frac{L_{N_x}^4 t^5}{5!} + \cdots \right] \dot{\boldsymbol{P}}_0,$$

and then add the two formulas:

$$\boldsymbol{P}_t = 2\boldsymbol{P}_0 - \boldsymbol{P}_{-t} - L_{N_x}^2 t^2 \boldsymbol{P}_0 + \frac{L_{N_x}^4 t^4}{12} \boldsymbol{P}_0 + \cdots \tag{5.2.2}$$

Depending on how many terms are retained one obtains finite- differences schemes of different orders.

2^{nd} *Order.* Retain the first three terms on the right hand side of (5.2.2),

$$\boldsymbol{P}_t = 2\boldsymbol{P}_0 - \boldsymbol{P}_{-t} - L_{N_x}^2 t^2 \boldsymbol{P}_0$$

or in the 1D case,

$$\boldsymbol{P}_t = 2\boldsymbol{P}_0 - \boldsymbol{P}_{-t} + c^2 t^2 \frac{\partial^2 \boldsymbol{P}_0}{\partial x^2}$$

which is the known central finite-difference formula when the time step size $\mathrm{d}t$ is used instead of t.

4^{th} *Order.* Retain the first four terms:

$$\boldsymbol{P}_t = 2\boldsymbol{P}_0 - \boldsymbol{P}_{-t} + c^2 t^2 \frac{\partial^2 \boldsymbol{P}_0}{\partial x^2} + \frac{t^4}{12} c^2 \frac{\partial^2}{\partial x^2} \left(c^2 \frac{\partial^2 \boldsymbol{P}_0}{\partial x^2} \right)$$

which is a fourth order scheme suggested by Dublain (1986). This scheme appears to be an improvement over 2nd order differencing. It does require twice as many spatial derivatives per time step, but the time step can be twice as large while maintaining improved accuracy.

5.3. Finite difference schemes derived from system

We now consider schemes derived from the Taylor expansion:

$$e^{G_n t} = I + G_n t + \frac{1}{2}(G_n t)^2 + \frac{1}{3!}(G_n t)^3 + \cdots.$$

We get:

$$\boldsymbol{V}_t = e^{G_n t}\,\boldsymbol{V}_0 = \boldsymbol{V}_0 + tG_n\boldsymbol{V}_0 + \frac{t^2}{2}G_n^2\boldsymbol{V}_0 + \frac{t^3}{3!}G_n^3\boldsymbol{V}_0 + \cdots$$

Truncation of this equation gives schemes of different orders. This method is often called the Taylor method in the literature. Retaining terms up to 4th order yields a scheme which gives results very similar to the 4th order Runge-Kutta scheme.

In a second order scheme two function evaluations are required per step (e.g. $G_n\boldsymbol{V}_0$ and $G_n^2\boldsymbol{V}_0 = G_n(G_n\boldsymbol{V}_0)$) as opposed to one function evaluation required for the 2nd order FD scheme above. A more efficient scheme can be derived by writing the above equation for time $-t$:

$$\boldsymbol{V}_{-t} = e^{-G_n t}\,\boldsymbol{V}_0 = \boldsymbol{V}_0 - tG_n\boldsymbol{V}_0 + \frac{t^2}{2}G_n^2\boldsymbol{V}_0 + \cdots,$$

and subtracting the two equations while retaining only the first term on the r.h.s. . This gives:

$$\boldsymbol{V}_t = \boldsymbol{V}_{-t} + 2tG_n\boldsymbol{V}_0.$$

Writing this equation in full yields:

$$\begin{bmatrix} P \\ \frac{\partial P}{\partial t} \end{bmatrix}_t = \begin{bmatrix} P \\ \frac{\partial P}{\partial t} \end{bmatrix}_{-t} + 2t \begin{bmatrix} 0 & 1 \\ c^2\frac{\partial^2}{\partial x^2} & 0 \end{bmatrix} \begin{bmatrix} P \\ \frac{\partial P}{\partial t} \end{bmatrix}_0$$

Elimination of $\partial P/\partial t$ from this system yields the single equation

$$P_{2t} = 2P_0 - P_{-2t} + 4C^2t^2\frac{\partial^2 P_0}{\partial x^2}.$$

This formula which spans two time steps has only half the efficiency as the scheme derived directly from the acoustic wave equations. In other words, here we would need to use $\alpha = c\,\mathrm{d}t/\mathrm{d}x = 0.1$ to get the same accuracy as the other scheme has for $\alpha = 0.2$.

5.4. The rem approach (rapid expansion method)

We have seen that finite-difference schemes derived directly from the acoustic wave equation are twice as efficient as schemes derived from the system

$$\frac{\partial \boldsymbol{V}}{\partial t} = G_n\boldsymbol{V}$$

The same type of improvement can be obtained over the Tal-Ezer method when the point of departure is the original acoustic wave equation instead of the coupled system (5.1.5). Consider first the homogeneous case:

$$\frac{\partial^2 \boldsymbol{P}}{\partial t^2} = -L_{N_x}^2\boldsymbol{P}. \tag{5.4.1}$$

We have seen that the formal solution to this equation is given by:

$$\boldsymbol{P}_t = \cos[L_{N_x}t]\boldsymbol{P}_0 + \frac{\sin[L_{N_x}t]}{L_{N_x}}\dot{\boldsymbol{P}}_0.$$

We now add to this solution the formal solution at time $-t$ and obtain:

$$\boldsymbol{P}_t = -P_{-t} + 2\cos[L_{N_x}t]\boldsymbol{P}_0. \tag{5.4.2}$$

However,

$$\cos[L_{N_x}t] = \frac{1}{2}\left[e^{iL_{N_x}t} + e^{-iL_{N_x}t}\right]$$

and

$$e^{iL_{N_x}t} = \sum_{k=0}^{M} C_k J_k(tR) Q_k\left(\frac{iL_{N_x}}{R}\right)$$

also,

$$e^{-iL_{N_x}t} = \sum_{k=0}^{M} C_k J_k(tR) Q_k\left(\frac{-iL_{N_x}}{R}\right)$$

Therefore,

$$\cos[\mathrm{i}L_{N_x}t] = \sum_{k=0}^{M/2} C_{2k} J_{2k}(tR) Q_{2k}\left(\frac{\mathrm{i}L_{N_x}}{R}\right)$$

($Q_k(y)$ are even functions of y for even k, and odd functions of y for odd k). This sum contains only even order functions Q_{2k} in contrast to the original Tal-Ezer method. Therefore the amount of computation will be half as well. Moreover, $Q_k\,(\mathrm{i}L_{N_x}/R)$ for even k contains only powers of $-L_{N_x}^2$ which is our basic operator $c^2(\partial^2/\partial x^2)$ (had we needed to evaluate for example $L_{N_x}^3$ this could have been more complicated). Now we need a recursion relation for Q_k with only even terms. Considering again the recursion relation:

$$Q_{k+1} = Q_{k-1} + 2\omega Q_k \tag{5.4.3}$$

we get:

$$\omega Q_k = \frac{Q_{k+1} - Q_{k-1}}{2}$$

Therefore,

$$\omega Q_{k+1} = \frac{Q_{k+2} - Q_k}{2}$$

$$\omega Q_{k-1} = \frac{Q_k - Q_{k-2}}{2}$$

Substituting the above into (5.4.3) multiplied by ω gives:

$$\frac{Q_{k+2} - Q_k}{2} = \frac{Q_k - Q_{k-2}}{2} + 2\omega^2 Q_k$$

or,

$$Q_{k+2} = (4\omega^2 + 2)Q_k - Q_{k-2}. \tag{5.4.4}$$

This equation allows recursion among even terms or odd terms separately. The recursion for even terms can be started by noting that $Q_0 = 1$ and $Q_2 = 1+2\omega^2$. For odd terms $Q_1 = \omega$ and $Q_3 = 4\omega^3+3\omega$. Putting $-L_{N_x}^2/R$ instead of ω^2 allows use of REM approach in a very similar manner to Tal-Ezer's method. However, values of P_{-t} and P_0 need to be known to initialize the process.

5.5. Solution for the source term

The formal solution with the source term is given by.

$$\boldsymbol{P}(t) = \left[\int_0^t \frac{\sin(L_{N_x}\tau)}{L_{N_x}} h(t-\tau)\,\mathrm{d}\tau\right] \boldsymbol{S}(x). \tag{5.5.1}$$

As in the previous section, it can be shown that:

$$\mathrm{i}\sin(L_{N_x}t) = \sum_{k=0}^{\infty} J_{2k+1}(tR) Q_{2k+1}\left(\frac{\mathrm{i}L_{N_x}}{R}\right) \tag{5.5.2}$$

Therefore,

$$\frac{\sin(L_{N_x}t)}{L_{N_x}} = \sum_{k=0}^{\infty} \frac{J_{2k+1}(tR)}{R} \frac{R}{\mathrm{i}L_{N_x}} Q_{2k+1}\left(\frac{\mathrm{i}L_{N_x}}{R}\right)$$

The summation will again contain only powers of the basic operator $-L_{N_x}^2$. A substitution in (5.5.1) gives:

$$\boldsymbol{P}(t) = \sum_k \left[\int_0^t \frac{J_{2k+1}(\tau R)}{R} h(t-\tau)\,\mathrm{d}\tau\right] \frac{R}{\mathrm{i}L_{N_x}} Q_{2k+1}\left(\frac{\mathrm{i}L_{N_x}}{R}\right) \boldsymbol{S}(x)$$

or

$$\boldsymbol{P}(t) = \sum_{2k+1} b_{2k+1} \frac{R}{\mathrm{i}L_{N_x}} Q_{2k+1}\left(\frac{\mathrm{i}L_{N_x}}{R}\right) \boldsymbol{S}(x) \tag{5.5.3}$$

with

$$b_k = \int_0^t \frac{J_k(\tau R) h(t-\tau)}{R}\,\mathrm{d}\tau. \tag{5.5.4}$$

b_k can be evaluated numerically as in the ordinary Tal-Ezer method. The recursion is initiated by:

$$\frac{R}{\mathrm{i}L_{N_x}} Q_1\left(\frac{\mathrm{i}L_{N_x}}{R}\right) \boldsymbol{S}(x) = \boldsymbol{S}(x),$$

and,

$$\frac{R}{\mathrm{i}L_{N_x}} Q_3\left(\frac{\mathrm{i}L_{N_x}}{R}\right) \boldsymbol{S}(x) = \left(2I - \frac{4L_{N_x}^2}{R^2}\right) \boldsymbol{S}(x) = 2\boldsymbol{S}(x) + \frac{4}{R^2} c^2 \frac{\partial^2 \boldsymbol{S}}{\partial x^2}$$

It can then be carried out by:

$$\left(\frac{R}{\mathrm{i}L_{N_x}}\right) Q_{k+2}\boldsymbol{S}(x) = \left(\frac{R}{\mathrm{i}L_{N_x}}\right) Q_k\boldsymbol{S}(x) - \left(\frac{R}{\mathrm{i}L_{N_x}}\right) Q_{k-2}\boldsymbol{S}(x) \quad (5.5.6)$$

5.6. Amount of work for REM

The amount of work for the REM is about $Rt/2$. Since $R = \pi c/\,\mathrm{d}x$ for 1D, the amount of work for propagating 100 grid points will be

$$1.1 \cdot \frac{\pi c}{\mathrm{d}x} \cdot \frac{100\,\mathrm{d}x}{2c} = 1.1 \cdot 50\pi = 165.$$

where the factor 1.1 was added to assure convergence (the expansion region should be slightly larger than Rt. For 2D and 3D the corresponding values will be 233 and 285. These numbers are significantly less than the corresponding numbers for second order finite-differences.

In terms of storage we need global variables for Q_k, Q_{k+2}, P_t and c^2. This is the same number of variables as are required for finite-differences. However, more space is required for storing time sections and snapshots which need to be in memory until all the terms in the recursion have been calculated.

5.7. Nonreflecting boundary conditions

For the REM approach we have not yet found a rigorous manner to introduce absorbing boundaries. However, we have found that by multiplying Q_k and Q_{k+2} in a strip surrounding the boundaries by a factor less than 1 we could almost eliminate all boundary reflections and wraparound. This procedure is similar to that of the temporal differencing case (Cerjan et al.,1985) except that here it is not clear how to justify this procedure on the basis of a differential equation.

5.8. Concluding remarks

We have presented an approach for modeling acoustic and elastic wave propagation in the Earth which we have developed. It appears that for realistic typical reflection seismology configurations, computer simulation can be performed in 2D and 3D. However, there are a number of areas where further research is required. One topic is the incorporation of a more complete material rheology which will include anisotropy and attenuation. First steps in that direction have been taken (Carcione et. al., 1988a,b). A second area in which there is room for improvement is the free surface boundary condition in the elastic simulations and in general handling more complicated geometries with spectral methods. A promising approach appears to be use of the non periodic Chebychev expansion instead of the Fourier expansion (Kosloff et al.,1989).

References

Baysal, E., Kosloff, D. and Sherwood, J., A nonreflecting two way acoustic wave equation, Geophysics, Vol 49, No 2, 1984.

Bracewell, The Fourier transform and its applications, McGraw Hill book company, 1978.

Carcione J.M., Kosloff D. and Kosloff R., Viscoacoustic wave propagation simulation in the Earth, Geophysics, 53, 769-777, 1988.

Carcione J.M., Kosloff D. and Kosloff R., Wave propagation simulation in a linear viscoacoustic medium, Geophys. Jour., 93, 393-407, 1988.

Cerjan, C., Kosloff D., Kosloff R. and Reshef M., A non reflecting boundary condition for discrete acoustic and elastic wave equations, Geophysics, 50, 705-708, 1985.

Clayton R., and Enquist B., Absorbing boundary condition for acoustic and elastic wave equations, Bull. Seis. Soc. Amer., 67, 1529-1540, 1977.

Dublain M.A., The application of high-order differencing to the scalar wave equation, Geophysics, 51, 54-66, 1986.

Gazdag J., Modeling of the acoustic wave equation with transform methods, Geophysics, 39, 885, 1988.

Hamming, R., Numerical methods for scientists and engineers. McGraw- Hill book company, 1978.

Kosloff D., Frazier G.A., Treatment of hourglass modes in low order finite element codes, Int. J. for numerical and analytical methods in Geomechanics 25, 7-72, 1977.

Kosloff D. and Baysal E., Forward modeling by a Fourier method, Geophysics, 47, 1402-1412, 1982.

Kosloff D., Reshef M. and Loewenthal D., Elastic wave calculations by the Fourier method. Bull. Seis. Soc. Amer. 74, 875-891, 1984.

Kosloff, R. and Kosloff D., Absorbing boundaries for wave propagation problems. Journal of Computational Physics, 63, 363-376. 1986.

Kosloff D., and Kessler D., Accurate depth migration by a generalized phase shift method, Geophysics, 52, 1074-1084, 1987.

Kosloff D., and Kessler D., Queiroz, A.F., Tessmer, E., Behle, E., and Strahilevitz, R., Solutions of the equations of dynamic elasticity by a Chebychev spec-

tral method. Submitted to Geophysics, 1989.
Levander A. R., Fourth-order finite-difference P - SV seismograms. Geophysics Vol 53 No 11, 1987.
Mora P., Personal communications, 1988.
Tal Ezer H., PhD. thesis, Tel Aviv University, 1984.
Virieux J., SH wave propagation in heterogeneous media: velocity stress finite-difference method, Geophysics, 49, 1933-1957, 1984.
Virieux J., P-SV wave propagation in heterogeneous media: velocity stress finite-difference method, Geophysics, 51, 889-901, 1986.
Zienkiewitz O.C., The finite element method, McGraw hill book company, 1977.